sEEGnal: an automated EEG preprocessing pipeline evaluated against expert-driven preprocessing

Federico Ramírez-Toraño[1]*, Christoffer Hatlestad-Hall[2], Ainar Drews[3], Hanna Renvall[4,5], Paolo María Rossini[6], Camillo Marra[7,8], Ira H. Haraldsen[2], Fernando Maestu[1,9,10], Ricardo Bruña[1,11,] * #.

1. Center for Cognitive and Computational Neuroscience, Universidad Complutense de Madrid, Madrid, Spain.
2. Department of Neurology, Oslo University Hospital, Oslo, Norway.
3. University of Oslo, UiO: Management and Support Units, IT Departement.
4. BioMag Laboratory, HUS Medical Imaging Centre, Helsinki University Hospital, Helsinki University and Aalto University School of Science, Helsinki, Finland
5. Department of Neuroscience and Biomedical Engineering, Aalto University, Helsinki, Finland.
6. Department of Neuroscience and Neurorehabilitation, IRCCS San Raffaele, Rome, Italy.
7. Memory Clinic, Fondazione Policlinico Universitario Agostino Gemelli IRCCS, Rome, Italy.
8. Department of Psychology, Catholic University of the Sacred Heart, Rome, Italy.
9. Department of Experimental Psychology, Cognitive Psychology and Speech & Language Therapy, Complutense University of Madrid, Madrid, Spain.
10. Health Research Institute of the Hospital Clínico San Carlos (IdISSC), Madrid, Spain.
11. Department of Radiology, Complutense University of Madrid, Madrid, Spain.

Corresponding author Ricardo Bruña ricardo.bruna@ucm.es

*These authors contributed equally to the work.

Abstract

Electroencephalography (EEG) preprocessing is a critical yet time-consuming step that often relies on expert-driven, semi-automatic pipelines, limiting scalability and reproducibility across large datasets. In this work, we present sEEGnal, a fully automated and modular pipeline for EEG preprocessing designed to produce outputs comparable to expert-driven analyses while ensuring consistency and computational efficiency. The pipeline integrates three main modules: data standardization following the EEG extension of the Brain Imaging Data Structure (BIDS), bad channel detection, and artifact identification, combining physiologically grounded criteria with independent component analysis and ICLabel-based classification.

Performance was evaluated against manual preprocessing performed by EEG experts at two complementary levels: preprocessing metadata (bad channels, artifact duration, and rejected components) and EEG-derived measures. In addition, test–retest analyses were conducted to assess the stability of the pipeline across repeated recordings.

Results show that sEEGnal achieves performance comparable to expert-driven preprocessing while preserving key neurophysiological features. Furthermore, the pipeline demonstrates reduced variability and increased consistency compared to human experts. These findings support sEEGnal as a robust and scalable solution for automated EEG preprocessing in both research and large-scale applications.

Keywords

EEG preprocessing, Automated pipeline, BIDS, Bad channel detection, Artifact detection

Highlights

Fully automated and modular EEG preprocessing pipeline.

Benchmarked against expert-driven preprocessing.

Comparable performance in metadata and EEG-derived measures.

Demonstrates stable performance in test–retest recordings.

BIDS-based framework for reproducible EEG data handling.

1. Introduction

Electroencephalography (EEG) is a non-invasive neuroimaging technique that measures the spontaneous electrical activity of the brain using a set of electrodes placed on the scalp[1]. The standard EEG setup typically includes a cap with integrated electrodes, digital amplifiers, and a software for data processing and visualization[2]. Compared to other noteworthy neuroimaging techniques, EEG presents some vital advantages: high temporal resolution; fair spatial resolution with the modern high-density EEG setups; portability; significantly lower hardware and consumables expenses; non-invasiveness; and no radiation[3]. As a result, modern EEG has become one of the most promising neuroimaging techniques for aiding in the diagnostics of neurological disorders, characterizing mood disorders and mental conditions, and revealing and defining the neurophysiological underpinnings of human cognitive functions.

Importantly, the raw EEG signal captures not only neuronal activity related to brain functions, but also physiological artefacts originating from blinks and eyes movements, heartbeats, and body movements. Additionally, it captures non-physiological artefacts induced by electronic noise and alternating current (AC) power lines[4]. A “pre-processing” pipeline is a set of methods applied to EEG recordings to remove (or at least minimise) the effects of such artefacts, keeping the desired brain activity unaffected. The pre-processing pipeline is an indispensable step before analysing EEG recordings in order to obtain valid results. Although there are general guidelines[5,6], they must be adapted to suit each specific experiment or condition.

The most common approaches of EEG pre-processing involve semiautomatic pipelines supervised by EEG experts. These approaches assure the quality of the pre-processed EEG data but present some considerable challenges in large-scale data analysis settings: the process presents an unaffordable time-consuming nature; the outcomes are strongly dependent on the expert who has performed the analysis; and, due to the dependence of the solutions on programming frameworks (mainly MATLAB and Python), the approaches are only suitable for field experts with some level of programming skills. In response to these limitations, several automated pipelines have been proposed, typically prioritizing either standardized preprocessing workflows or data-driven artefact detection

strategies. However, many of these approaches do not explicitly integrate both perspectives within a unified and interpretable framework.

sEEGnal is defined in separate modules, namely standardization, bad channel detection, and artifact identification. The standardization module is based on the EEG extension of the BIDS framework[7] to ensure structured, interoperable, and reproducible data handling. The bad channel detection and artifact detection modules combine physiologically grounded criteria with ICA-based decomposition. This design enables a transparent and modular preprocessing workflow that aligns with expert practices while facilitating scalability across datasets. Importantly, we evaluate sEEGnal against manual preprocessing performed independently by multiple EEG experts, allowing performance to be interpreted in the context of expert-driven variability. Given the absence of ground truth in real-world EEG data, performance is assessed at two complementary levels: preprocessing metadata (e.g., bad channels, artefact duration, and rejected components) and EEG-derived measures. We assess the impact of preprocessing on downstream signal properties, including power spectral density and functional connectivity, as well as the stability of the pipeline across repeated recordings within the same session. Together, these analyses provide a structured and multi-level validation of the proposed approach.

2. sEEGnal overview

The main characteristics of sEEGnal can be summarized as follows:

- Comprehensive. We have defined the algorithm underneath sEEGnal following widely accepted guidelines for EEG experiments[5,6]. The workflows and parameters associated with each module have been designed to obtain the best performance regarding outcomes while keeping time and memory consumption in mind.
- Automatic. We have designed sEEGnal to be completely automated, using a pre-defined configuration. At any moment, the user may change at convenience the configuration parameters stored in the corresponding JSON files.
- Comparable to human EEG experts. We have designed sEEGnal to match the performance of a human EEG expert, which is widely recognized as the current gold standard for EEG pre-processing.

- Time and memory efficient. We have developed sEEGnal to work on large datasets. To this end, in addition to its automatic nature, the efficiency in the use of resources (i.e., efficiency in computational and memory use) is vital.
- Open-Source. We have designed sEEGnal as an open-source tool, enabling free and unrestricted use within the community. The majority of the codebase is implemented in Python, while two modules are written in C++ to ensure adequate computational performance. We have developed sEEGnal in Python 3.12.10 and builds upon the MNE-Python framework[8]. A complete list of dependencies is provided in the Supplementary Material.

The following sub-sections deepens in the high-level modules comprising sEEGnal: standardisation, bad channels identification, and artefact detection.

2.1. Standardisation

To facilitate the creation and distribution of public EEG datasets, and interoperability with concurrent EEG pre-processing and analysis frameworks, the first module focuses on the standardisation of the data following the EEG extension of the BIDS standard[7]. BIDS defines a consistent protocol for folder structure, filenames, metadata, and file formats to store several types of neuroimaging data (as well as other related information), including EEG, magnetoencephalography (MEG) and other neuroimaging data. An overview of the BIDS structure used in this pipeline is provided in the Supplementary Material.

2.2. Bad channel detection

Under our rationale, a bad channel refers to an electrode whose signal is unreliable due to technical issues rather than reflecting physiological brain activity. Neural signals tend to spread across electrodes because of volume conduction, resulting in spatially correlated patterns. In contrast, noise arising from electrode malfunction, poor contact, or hardware-related problems is often spatially isolated and does not propagate to neighbouring channels. Therefore, the identification of bad channels relies on detecting signals that deviate from the expected spatial and statistical structure of the EEG recording. Following this rationale, our pipeline defines bad channels as those exhibiting abnormal signal characteristics relative to the rest of the recording, including indicators

of poor electrode contact, non-physiological amplitude, spectral abnormalities, artificial inter-channel coupling, or excessive variance:

- High impedance. The impedance between the skin and the electrode is a fast and accessible proxy for data quality, but only in conjunction with other metrics[9]. sEEGnal marks as bad those channels which impedance surpasses a predefined value. This value is configurable by the user through the JSON configuration files, with the default value set to 200 kΩ (see Supplementary Material).
- Impossible amplitude. The impossible amplitude refers to channels with low or high amplitudes that physiologically cannot reflect to brain signals. sEEGnal estimates the standard deviation of each channel and those channels with standard deviations outside a lower and upper thresholds are marked as bad. The lower and upper values are configurable by the user through the JSON configuration files, with the default values set to 1 µV and 500 µV.
- Power spectrum. An abnormal power spectrum between 45 and 55 Hz is a robust measure to detect possible bad channels (see Supplementary Material). First, sEEGnal estimates each channel's power spectrum between 45 and 55 Hz using the Welch method. Then, for each channel, sEEGnal estimates the average power spectrum of the EEG recording excluding the current channel and compare the value of the current channel with the value of the rest of channels. sEEGnal marks as bad those channels with values 3 times greater than the average. This value is set by default but can be changed in the JSON configuration file.
- Gel bridges. A gel bridge occurs when conductive material (typically electrode gel) unintentionally connects two or more adjacent electrodes, creating an artificial and abnormal low-impedance pathway between them. This bridging causes the affected electrodes to record highly correlated or nearly identical signals[10]. sEEGnal estimates both the physical distance between each pair channels and the correlation coefficients of their data. All pairs of channels closer than 5 cm (the average distance between neighbouring sensors of the montages used for this study) that presents correlations above 0.999 are marked as bad channels. These values are set by default but can be changed in the JSON configuration file.

- **High amplitude variance**. Channels that present abnormal amplitude standard deviation when compared to the rest of the EEG channels are very likely bad channels. First, sEEGnal estimates each channel's standard deviation. Then, for each channel, sEEGnal estimates the average standard deviation of the EEG recording excluding the current channel and compare the value of the current channel with the value of the rest of channels. sEEGnal marks as bad those channels with values 10 times greater than the average. This value is set by default but can be changed in the JSON configuration file.

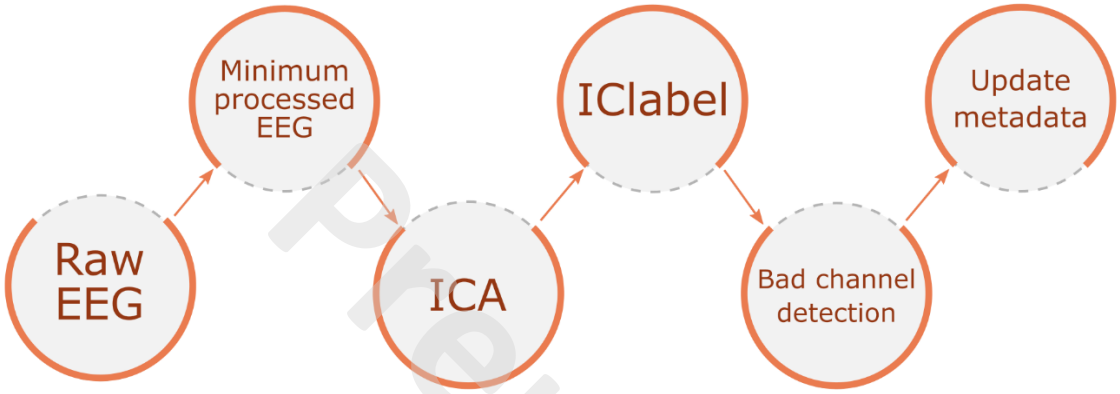

Figure 1. Sub-modules in Bad channel detection module. Abbreviations: ICA, independent component analysis.

The workflow of the module is presented Figure 1 and described as follow:

1. Load the raw EEG recording.
2. Apply a minimum pre-processing to the EEG recording to fulfil the IClabel[11] requirements: a bandpass filter between 1 to 100 Hz; a downsample to 500 Hz; notch filter centred in 50 Hz; the transformation to 4-seconds epochs. No epochs were removed in this step.
3. Decompose the minimum-pre-processed EEG data into Independent Components (ICs) using a Second Order Blind Identification (SOBI) algorithm and classified them using ICLabel.
4. Apply the bad channel criteria stepwise in the following order: high impedance, physiologically unattainable amplitude, power spectrum, gel bridges, and high variance. Channels marked as bad by a criterion are excluded from subsequent criterion evaluations.

5. Update the metadata accordingly to the results.

2.3. Artefact detection

This module aims to identify artefacts present on EEG recordings, i.e. defining the onset and duration of the artefact. Specifically, eye-related, muscle-related, sensor-related artefacts, and others[12]:

- Eye-related artefacts. Eye-related artefacts arise primarily from electrooculographic (EOG) activity generated by eye blinks, vertical and horizontal eye movements, and eyelid flutter. These movements produce large-amplitude deflections that typically dominate the EEG below approximately 2–4 Hz, with maximal expression in frontal and frontopolar electrodes. To detect these artefacts, sEEGnal filters the EEG time series between 1 and 5 Hz and divided it into frontal channels and “background” channels. sEEGnal estimates the average standard deviation of both groups, and it looks for peaks in the frontal group with amplitudes at least 10 times greater than the “background” group. Finally, sEEGnal merges all the peaks to create the ocular artefacts. The threshold and the frequency limits are set by default but can be changed in the JSON configuration file.
- Muscle-related artefacts. Muscle artifacts (EMG) arise from the contraction and mechanical tension of muscles located in proximity to the recording electrodes, producing electromyographic activity that contaminates the EEG signal. These artefacts exhibit a broad spectral distribution, extending from near 0 Hz to frequencies exceeding 200 Hz, and their amplitude and waveform morphology are strongly influenced by the intensity and duration of the underlying muscle activity. To detect these artefacts, sEEGnal reconstructs time series using the ICs marked as “muscle” by IClabel with a certainty threshold of 0.7. Then, sEEGnal filters the muscle time series for high frequencies between 110 to 145 Hz (a range commonly used as a heuristic for EMG artifact detection[8,13]), and, for each channel, sEEGnal looks for peaks whose amplitude were 10 times greater than the average amplitude of the channel. Finally, sEEGnal merges all the peaks temporally closer than 0.5 seconds to create the muscle artefacts. The frequency, the thresholds and the distance between peaks are set by default but can be changed in the JSON configuration file.

- Sensor-related artefacts. Sensor-related artifacts—commonly termed channel jumps, electrode pops, or impedance shifts—originate from abrupt changes in electrode–skin impedance or mechanical instability of the sensor or cable. These artifacts manifest as sudden, large-amplitude steps or transient bursts, often with no physiological correlates. Their spectral signature is broadband but irregular, frequently introducing atypical high-amplitude low-frequency energy (< 5 Hz) due to the step-like displacement in the time domain. To detect these artefacts, sEEGnal filters the EEG time series between 0.5 and 5 Hz. Then, for each channel, sEEGnal estimates the standard deviation of the channel, and sEEGnal looks for peaks with amplitudes that are 5 times greater than the standard deviation of the channel. The threshold and the frequency limits are set by default but can be changed in the JSON configuration file.
- Other artefacts. This category encompasses signal segments with amplitudes or morphologies that are incompatible with known neurophysiological processes yet cannot be confidently attributed to a specific artifact source. These episodes typically present as abrupt, high-amplitude transients or sustained deviations that exceed biologically plausible voltage ranges for scalp EEG. Although their characteristics suggest non-neural contamination—such as sudden impedance fluctuations, cable disturbances, or undocumented environmental interference—the precise origin remains indeterminate. To detect these artefacts, sEEGnal filters the EEG time series between 2 and 45 Hz. For each channel, sEEGnal looks for time points with impossible high amplitudes, i.e. time points where the amplitude was above 500 µV. The threshold and the frequency limits are set by default but can be changed in the JSON configuration file.

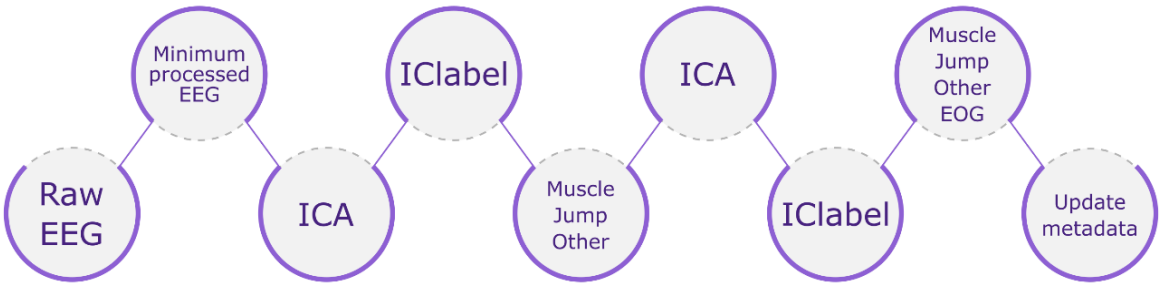

Figure 2. Sub-modules in Artifact detection module. Abbreviations: ICA, independent component analysis.

The workflow of the module is presented in Figure 2 and described as follow:

1. The raw EEG recording is loaded.
2. Apply a minimum pre-processing to the EEG recording to fulfil the IClabel[11] requirements: a bandpass filter between 1 to 100 Hz; a downsample to 500 Hz; notch filter centred in 50 Hz; the transformation to 4-seconds epochs. No epochs were removed in this step.
3. Decompose the minimum-pre-processed EEG data into Independent Components (ICs) using a Second Order Blind Identification (SOBI) algorithm and classified them using ICLabel.
4. Apply the artifact criteria stepwise for the following categories: muscle-related, sensor-related, and other.
5. Since muscle and sensor artifacts may dominate on the estimation of ICs, we perform a second IC estimations discarding epochs with artefacts.
6. Apply again the artifact criteria stepwise for the following categories: muscle-related, sensor-related, other, and eye-related.
7. Update the metadata accordingly to the results.

3. Material and Methods

Since there is neither an established gold standard for automated EEG pre-processing, nor a ground-truth associated to a real-world EEG recording, the quality assessment of an EEG pre-processing pipeline is not straightforward. To date, the best approach to evaluate the performance of an automatic EEG pre-processing pipeline is to consider EEG experts the gold standard and then compare the outcomes of the automatic tool with them. An overview of the process followed in this study to achieve our goal is presented in Figure 3.

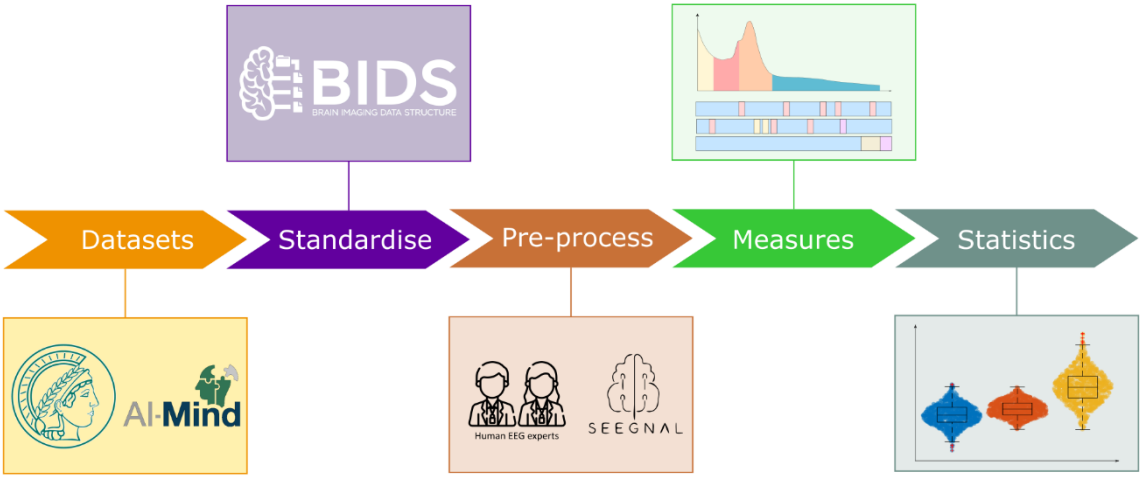

Figure 3. Overview of the pipeline followed in this study.

To use the EEG experts as gold standard in the comparison, we selected EEG datasets that fulfil two vital requirements: the recordings come from humans (not synthetic data), and the recordings have been manually pre-processed by EEG experts (or at least, visually inspected by them). In addition, we defined a comprehensive battery of outcomes to compare the performance of sEEGnal with the pre-processing by EEG experts.

We divided these outcomes into two conceptual categories, namely pre-processing metadata and EEG-derived measures. The pre-processing metadata refers to objective metrics of the EEG pre-processing, namely time and memory consumption, as well as the average number of bad channels, artefacts, and components rejected per EEG recording. As EEG-derived measures, we have selected two widely used EEG features, namely power spectrum and functional connectivity.

The pre-processing of both datasets and the performance assessment was done in a Windows 11 Education version 23H2 with a processor Intel® Core™ i7-3820 CPU @ 3.60GHz and 64 GB of RAM memory.

3.1. Datasets

For this study, we defined three datasets: the LEMON dataset, the AI-Mind dataset, and the test-retest dataset. These datasets include data from one public and one private source. Table 1 summarizes the number and types of EEG recordings in each dataset.

	N	Eyes closed	Eyes Open

LEMON dataset	20	10	10
AI-Mind dataset	20	10	10
Test-retest dataset	20	10 pairs	10 pairs

Table 1. Datasets used in the present study.

3.1.1. LEMON dataset

The "Leipzig Study for Mind-Body-Emotion Interactions" (LEMON)[14] is a publicly available dataset consisting of EEG recordings from 227 healthy participants comprising a young and an elderly group acquired cross-sectionally in Leipzig, Germany, between 2013 and 2015. For 216 of the participants, the creators recorded task-free (resting state) EEG using a BrainAmp MR plus amplifier in an electrically shielded and sound-attenuated EEG booth using a 62-channel (61 scalp electrodes plus 1 electrode recording the VEOG below the right eye) cap and active electrodes (actiCAP) (both Brain Products GmbH, Gilching, Germany) positioned according to the extended version or the international 10–20 system, (also known as 10-10 system), and referenced to FCz. The skin electrode impedance was kept below 5 KΩ. The EEGs were bandpass filtered online between 0.015 Hz and 1 kHz and digitized with a sampling rate of 2500 Hz. The EEG session included a total of 16 blocks, each 60 s long, 8 with eyes-closed (EC) and 8 with eyes-open (EO).

According to the database description, the raw EEG data was bandpass filtered between 1 and 45 Hz and downsampled to 250 Hz. Bad channels were rejected after visual inspection, looking for frequent jumps/shifts in voltage or poor signal quality. Data intervals containing extreme peak-to-peak deflections or large bursts of high frequency activity were identified by visual inspection and removed. Then, data was transferred to EEGLAB[15] (version 14.1.1b) for MATLAB. The dimensionality of the data was reduced using principal component analysis, by keeping the minimum number of components that explain 95% of the total data variance. Last, data was studied using the Infomax implementation (*runica*) of the independent component analysis[16] (ICA), and components reflecting eye movement, eye blinks, or heartbeat related artefacts were removed. Finally, data was segmented into 4-second epochs of clean data, plus 2 seconds of real data at each side, as padding.

For this study, we randomly selected 50 subjects resulting in 100 task-free EEG recordings (50 eyes-closed and 50 eyes-opened).

3.1.2. AI-Mind dataset

The AI-Mind dataset[17] is a private dataset of 1,022 participants within MCI continuum aged between 60 and 80 years, around 250 participants per each of the four involved countries (Spain, Italy, Norway and Finland). For all participants, two 5-minutes eyes-closed EEG and two 5-minutes eyes-open EEG were recorded. EEGs were recorded using 126 electrodes prewired in an elastic cap (ANT neuro WaveguardTM), in addition to two auxiliary electrodes placed below the left eye (electro-oculogram; EOG), and on the right clavicle bone (electrocardiogram; ECG). The electrodes were labelled according to the 10-5 system[18]. The impedances were kept as low as possible, preferably below 25 kΩ. The ground electrode was placed on the left mastoid, while the CPz electrode served as the online reference. The signals are amplified by an eego™ mylab EE-228 amplifier system and digitalized and stored using eego™ software, both provided by ANT neuro/eemagine Medical Imaging Solutions GmbH, Berlin, Germany. EEGs were recorded at a sampling rate of 2,000 Hz with an anti-aliasing filter with a high cut-off frequency of 520 Hz.

For the pre-processing, the EEG recordings were manually pre-processed by 4 EEG experts (including the main author of the paper Federico Ramírez-Toraño) from the Centre for Cognitive and Computational Neuroscience using Fieldtrip[13] in MATLAB. The first step in the pipeline is a visual inspection for bad channels and artefacts. Spatially complex artefacts such as muscle activity might dominate the blind source separation, so segments containing these artefacts must be excluded from this analysis. Then, data was studied using second order blind identification (SOBI)[19], and components associated to eye movements and heart beats were labelled and subtracted. After the component rejection, the data was again visually reviewed to confirm the artefacts present in the EEG recording. Finally, data was segmented into 4-second epochs of clean data, plus 2 seconds of real data at each side, as padding.

For this study, we randomly selected 20 subjects of the AI-Mind dataset. For each subject we selected one EEG recording, resulting in 20 task-free EEG recordings (10 eyes-closed and 10 eyes-opened).

3.1.3. Test-retest dataset

To perform consistency analysis, we created another dataset from a subset of the AI-Mind dataset. Specifically, from the AI-Mind dataset, another 20 subjects were randomly selected. Each subject has 4 EEG recordings (two eyes-closed resting and two eyes-opened) obtained during the same session in an interleaved fashion (eyes open, eyes closed, eyes open, eyes closed).

3.2. Performance measurements

3.2.1. Metadata

For each EEG recording and each of the conceptual modules defined in section 2, we stored the time used to perform the task and the peak memory consumed during the task. For sEEGnal we used the Python modules *time* and *tracemalloc*, respectively. For the EEG experts, we used the MATLAB functions *tic-toc* and *memory*, respectively.

In addition, we stored the number of bad channels, the total duration of artefacts, and ICs rejected.

3.2.2. Power spectrum

For each channel, the power spectrum was calculated by means of Welch's method using a Hann window of 4 seconds (this is, after removing the padding) and 0.25 Hz of spectral resolution. This method estimated the periodogram between 2 and 45 Hz for each epoch and then averaged across epochs. The relative power spectrum of each channel was obtained by normalizing the power spectrum by the total broadband power, resulting in a value ranging from 0 to 1. As a result, a 2D matrix (*number of channels x frequency steps*) was obtained for each recording and pre-processing approach.

3.2.3. Functional connectivity

Functional connectivity was estimated using the phase locking value (PLV)[20,21] for each classical frequency band (delta, theta, alpha, low beta, high beta, gamma)[22]. This measure is based on the hypothesis of *phase synchronization* for connected brain activity, i.e., that the instantaneous phase of two connected signals should evolve together, and, therefore, the difference between them should be bounded. According to how "locked"

this difference is through the EEG epoch, the PLV ranges from 0 to 1, where the lower bound indicates no connectivity and the upper full connectivity.

For each epoch, the signal was filtered in one of the classical bands, the padding was removed, and the PLV was estimated for each pair of channels. Finally, the PLV for the pair of channels was estimated as the average across epochs. As result, a 3D matrix (*number of channels x number of channels x frequency band*) was obtained for each recording and pre-processing approach.

3.3. Statistical analysis

The analysis performed in this study intend to evaluate two main aspects of the proposed solution: the performance of sEEGnal pipeline compared to a human-driven pipeline, and the consistency of the result between two recordings within the same session. A global overview of the statistical analysis is presented in Figure 4.

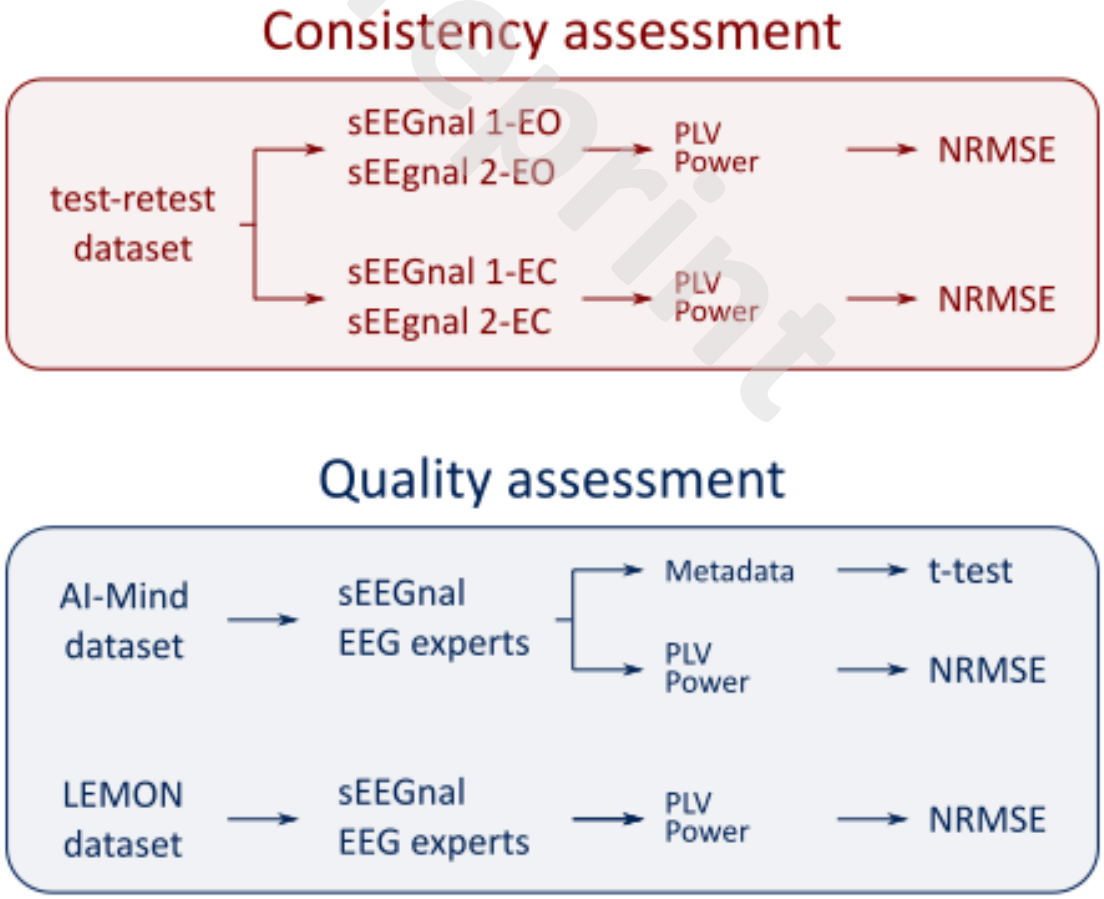

Figure 4. Global map of the analysis performed in this study. Abbreviations: PLV, phase locking value; NRMSE, normalised root mean squared error.

We assessed the difference between the number of bad channels detected, the total duration of the artefacts detected, pooled across all categories, and the ICs rejected by sEEGnal and the EEG experts by means of paired *t*-tests. In addition, the number of times each channel was marked as "bad" was estimated. Finally, we analysed the nature of artefacts (EOG, muscle, jump, other) as marked by sEEGnal and EEG experts. Due to the lack of metadata information regarding the LEMON dataset, only the AI-Mind dataset was used for the metadata analysis.

We assessed the quality of sEEGnal through the output measurements (power spectra and functional connectivity) using the normalized root mean squared error (NRMSE). NRMSE offers a dimensionless estimation of similarity between two measures:

$$RMSE = \sqrt{\frac{1}{N}\sum_{i=1}^{N}(measure_1[i] - measure_2[i])^2}$$

$$NRMSE = \frac{RMSE}{range(measure_{human})}$$

An NRMSE close to 0 indicates a high degree of similarity between the signals, while NRMSE close to 1 suggest differences comparable to the total magnitude of the signal.

To assess the consistency of sEEGnal, we estimated the NRMSE values for same-session EEG recordings from the Test-retest dataset. Specifically, for each subject and session, we compared the eyes-closed recordings and the eyes-opened task-free recordings separately.

To assess the performance of sEEGnal, we estimated the NRMSE between EEG recording from the AI-Mind dataset and LEMON dataset pre-processed either with sEEGnal or by EEG experts. Finally, to gain a comprehensive insight and detect any possible spatial or frequency bias, the NRMSE values were plotted for each sensor and frequency band.

For example, to compare the power spectrum after pre-processing by sEEGnal and an EEG expert, first, we loaded the power spectrum obtained from all the EEG recordings with the two pre-processing approaches. Second, we selected, from each recording, the desired frequency band and channel. Third, we estimated the NRMSE between the values for the specific frequency band and sensor pre-processed by sEEGnal and the EEG expert.

Finally, to obtain a visual insight of the spatial "quality map" the NRMSE values were averaged across recordings (Figure 5). For the sake of clarity, we present a pseudocode outlining the method in the Supplementary Material.

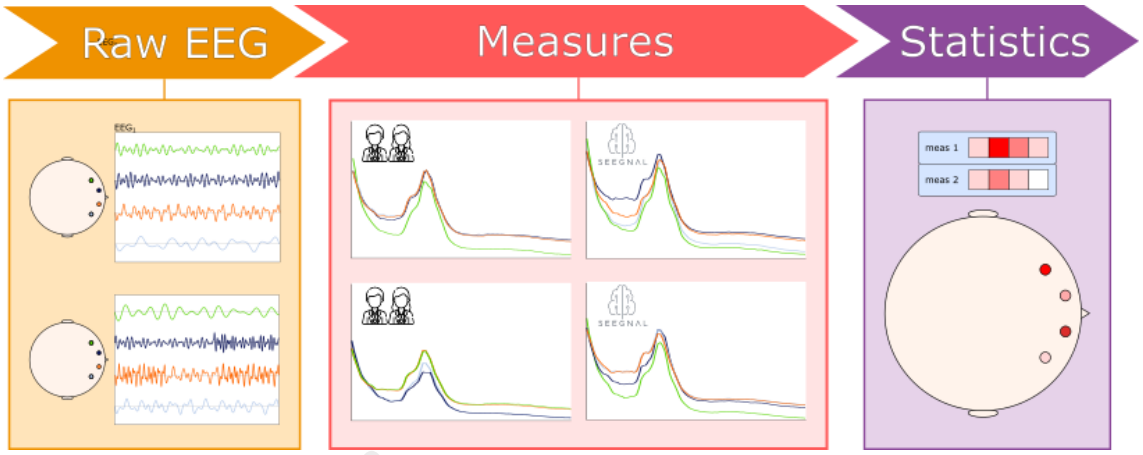

Figure 5. Pipeline to assess sEEGnal performance using the power spectrum. For the sake of clarity, this example is simplified by considering only two recordings, the frontal area, and one metric. The power spectra of frontal channels are estimated using the data obtained either by sEEGnal of the human EEG experts. The power spectra of each channel are compared using correlation and NRMSE, and the average is plot in head space for spatial visualization.

4. Results

4.1. Metadata

4.1.1. AI-Mind dataset

Table 2 presents the metadata results. Regarding time spent by each module, we observed similar average time in each conceptual module but greater standard deviation in the EEG experts. We observed less memory consumed by the proposed pipeline sEEGnal.

Regarding the number of bad channels, artefacts, and components rejected, we observed a similar performance with both pipelines.

Measure	Module	sEEGnal	EEG experts	p-value	Cohen's d
Time	Bad channel detection	324.40 (85.45)	372.55 (561.65)	0.710	0.173
	Artefact detection	373.52 (91.30)	425.70 (235.40)	0.318	0.470
Memory	Bad channel detection	2473.82 (620.89)	3134.19 (259.83)	<0.001	1.911
	Artefact detection	2399.50 (602.38)	-	-	-
# Bad channels		6.05 (3.41)	6.21 (3.59)	0.863	0.080
Artefacts in seconds		16.71 (17.61)	20.24 (19.48)	0.172	-0.650
# ICs rejected		2.10 (1.12)	1.82 (0.70)	0.239	-0.557

Table 2. Metadata measures regarding performance for EEG experts and for sEEGnal. Time is measured in seconds, Memory in Megabytes. The results are presented as mean (standard deviation). Due to a human mistake, the metadata regarding EEG expert memory in artefact detection is lost.

The spatial distribution of the bad channels is presented in Figure 6. For clarity purposes, the channel distribution was divided into groups according to the percentage of times the bad channel was marked as bad (from marked as bad in 45% of the recordings to 0 times marked as bad). First, we observed that the maximum proportion of recordings in which a channel was marked as bad reached 45% for sEEGnal, whereas it was 16% for human experts. The channels most frequently identified as bad by sEEGnal were predominantly located in frontal and temporal regions, a spatial pattern that was also observed in expert annotations.

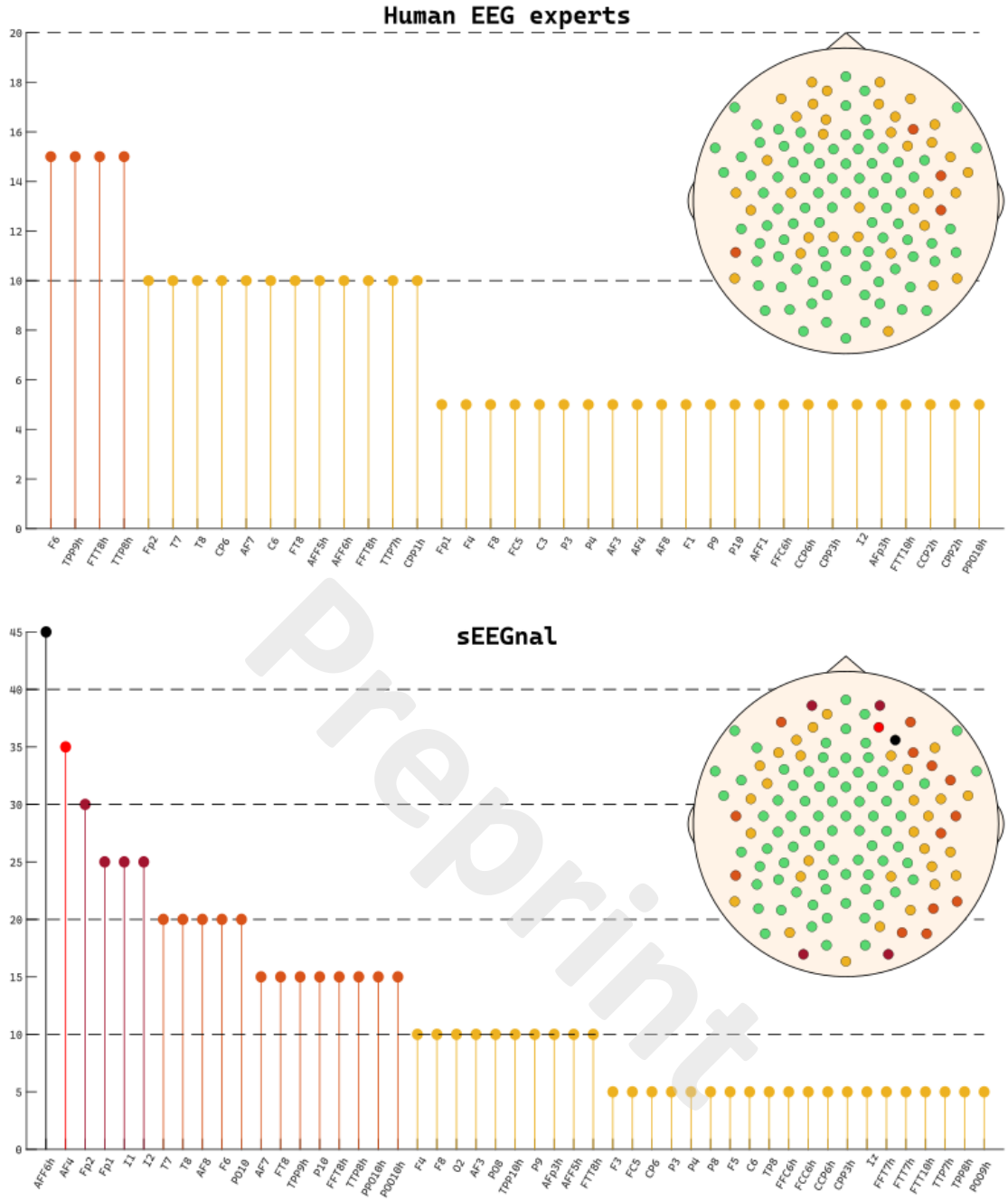

Figure 6. Spatial distribution of bad channels. On the top panel the information regarding the EEG experts. On the bottom panel the information regarding sEEGnal. The colormap divides the bad channels in groups according to their incidence in the EEG recordings pre-processed. For clarity purposes, the channel distribution was divided into groups according to the percentage of times the bad channel was marked as bad (from marked as bad in 45% of the recordings to 0 times marked as bad)

The types of ICs and the types of artefacts are presented in Figure 7. Regarding the ICs, 1,59% of the components were labelled for rejection by EEG experts, while 7,14% were labelled for rejection by sEEGnal. Regarding the types of artefacts, EEG experts classified

32,82% of the artefacts as eye-related, 21,02% as muscle-related, 39,85% as electronic jumps, and 6,32% as "other". For sEEGnal, 44,01% of the artefacts were eye-related, 36,94% muscle-related, 17,29% electronic jumps, and 1,76% "other". A chi-square test of homogeneity revealed significant differences in the distribution of artefact types between sEEGnal and EEG experts (χ^2 (3) = 124,57, p < ,001).

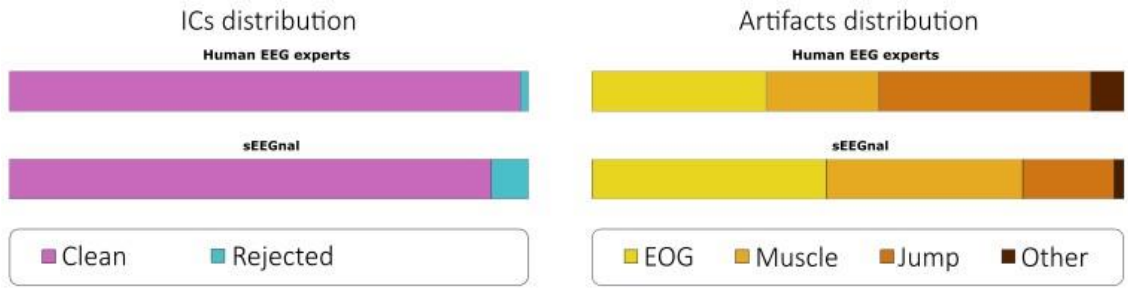

Figure 7 .Details of the ICs and artefacts present in the recordings. On the left, the distribution of ICs according to their type. On the right, the types of artefacts. Abbreviations: EOG, electrooculogram.

4.2. Power spectra

4.2.1. LEMON dataset

The power spectra obtained by sEEGnal showed a great resemblance to the ones averaged from the EEG experts (as an example, see Figure 8). For purposes of visualization, the power spectra obtained by both sEEGnal and the EEG experts are plotted in Figure 8 (top panel). The global resemblance is presented in Figure 8 (bottom panel), where the power of each frequency band obtained by sEEGnal for all subjects and channels are plotted against the ones obtained by the EEG experts.

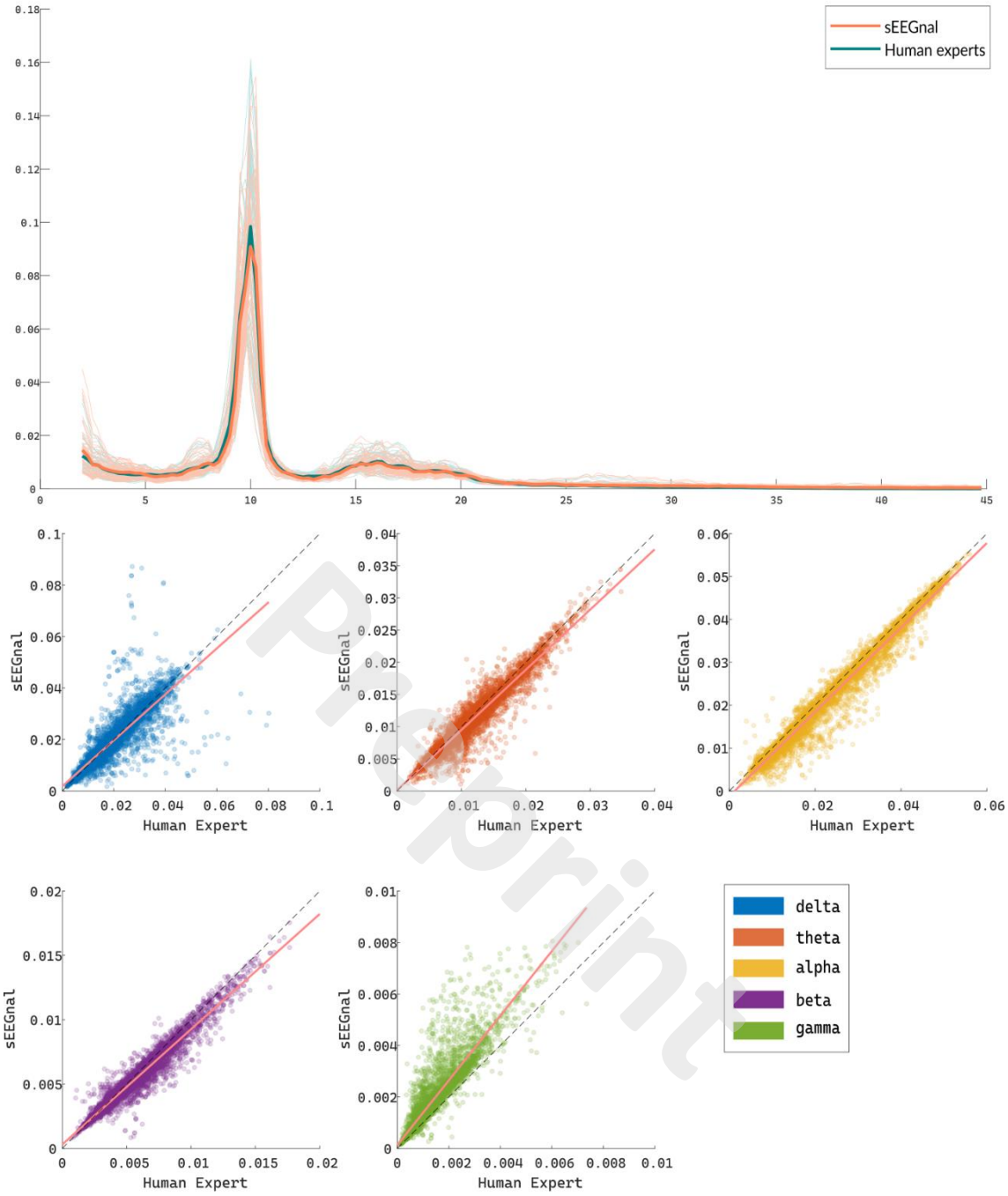

Figure 8. Comparison of power spectra obtained by the EEG experts and by sEEGnal in the LEMON dataset. On the top panel, the power spectra of a subject processed by sEEGnal and by EEG experts. The pale lines represent individual channels, and the solid lines represent the average power spectrum across channels for each preprocessing approach. On the bottom panel, an X-Y plot of the value obtained by sEEGnal and EEG expert dataset for the power in each band. The dash line represents a perfect correspondence (1:1), and the pink line represents the least-squares line.

Regarding the frequency bands, the NRMSE values for all channels in all recordings analysed are below 0.08, meaning the maximum difference across all the data analysed is

below 8% of the metric range, with the delta band being the one with larger differences. (Figure 9, top). Regarding the spatial distribution of the differences, the frontal channels in the delta band presented the highest differences, followed by the alpha band widespread across the head (Figure 9, bottom panel).

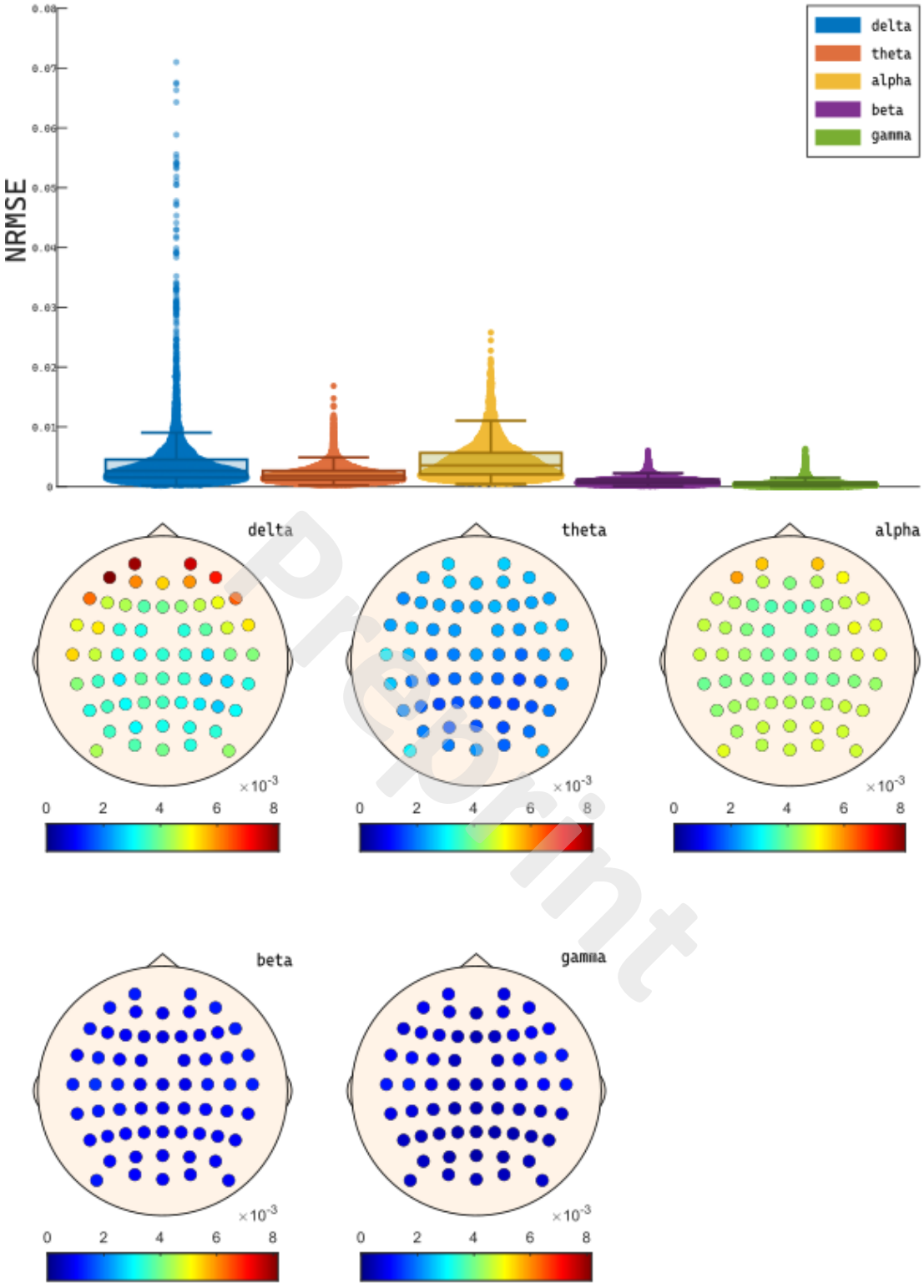

Figure 9. NRMSE values of the power spectra in the LEMON dataset. On the top panel, violin plots representing of the NRMSE distributions for all channels for each frequency band. On the bottom panels, spatial distribution of NRMSE values across the head for each frequency band. Abbreviations: NRMSE, normalised root mean square error.

4.2.2. AI-Mind dataset

The power spectra obtained by sEEGnal showed high resemblance to the ones averaged from the EEG experts (Figure 10). For purposes of visualization, the power spectra obtained by sEEGnal and the EEG experts are depicted in Figure 10 (top panel). The global resemblance is presented in Figure 10 (bottom panel), where the average power of each frequency band obtained by sEEGnal for all subjects and channels are plotted against the ones obtained by the EEG experts in an X-Y plot.

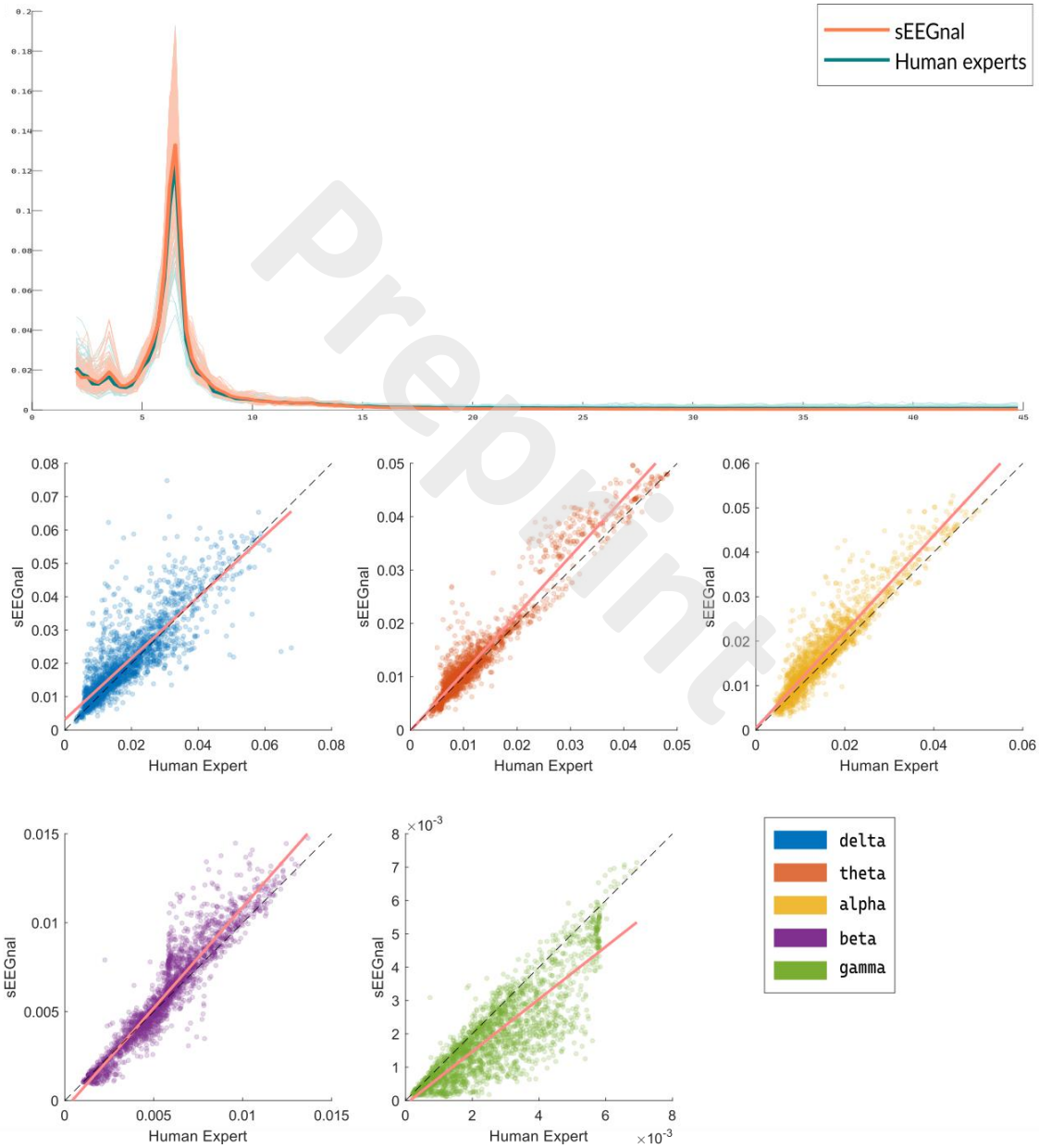

Figure 10. Comparison of power spectra obtained by the EEG experts and by sEEGnal in the AI-Mind dataset. On the top panel, the power spectra of a subject processed by sEEGnal and by EEG experts. The pale lines represent individual

channels, and the solid lines represent the average power spectrum across channels for each preprocessing approach. On the bottom panel, an X-Y plot of the value obtained by sEEGnal and EEG expert dataset for the power in each band. The dash line represents a perfect correspondence (1:1), and the pink line represents the least-squares line.

Regarding the power per frequency band, the NRMSE values for all channels in all recordings analysed are below 0.08, meaning the maximum difference across all the data analysed is below 8% of the metric range, with delta band being the one with more differences. (Figure 11, top). Regarding the spatial distribution of the differences, all channels present NRMSE values below 1,5% of the range of the metric (Figure 11, bottom panel), with the frontal channels in the delta band presenting the largest differences, followed, as in the case of the LEMON dataset, for the alpha band.

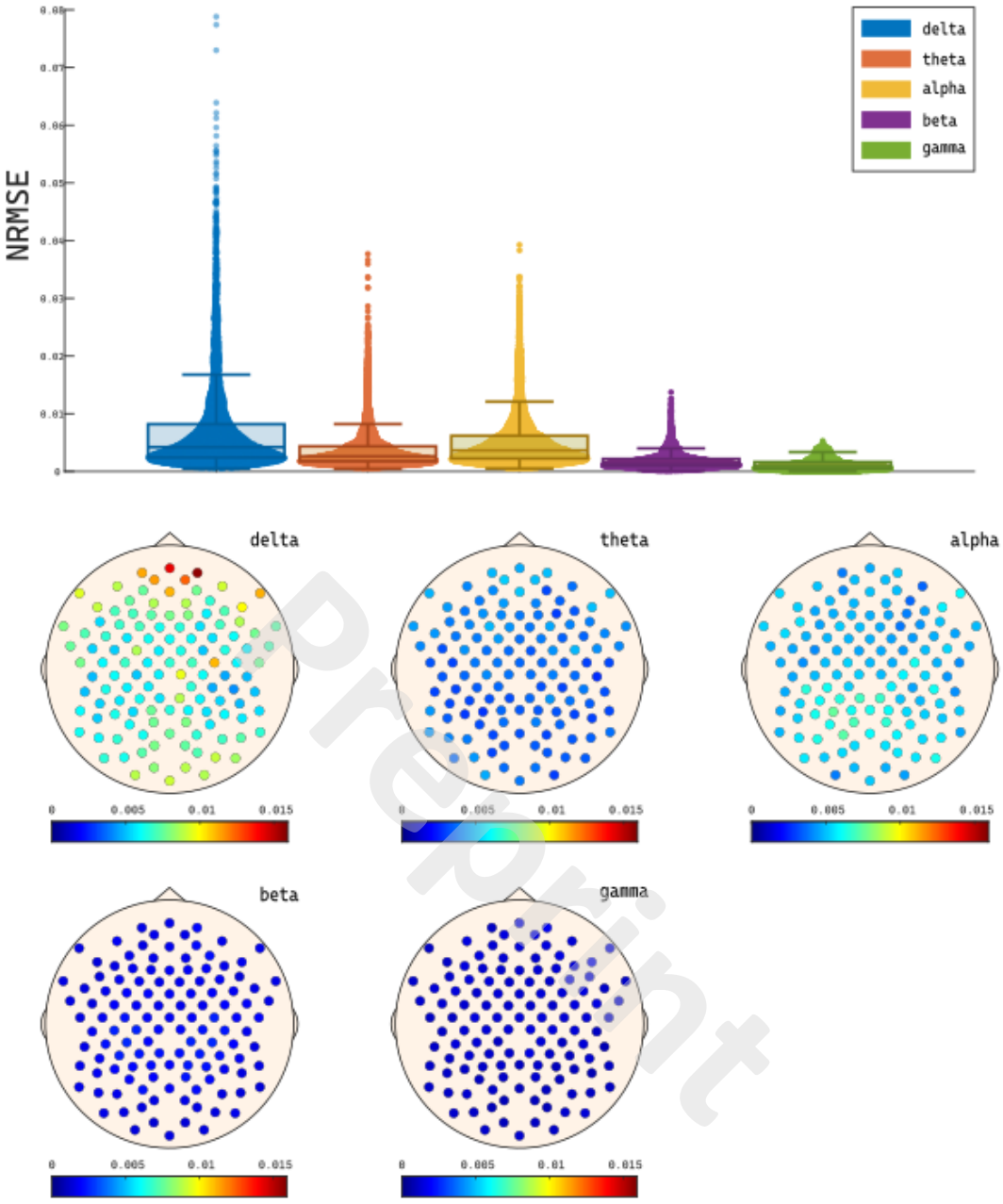

Figure 11. NRMSE values of the power spectra in the AI-Mind dataset. On the top panel, violin plots representing of the NRMSE distributions for all channels for each frequency band. On the bottom panels, spatial distribution of NRMSE values across the head for each frequency band. Abbreviations: NRMSE, normalised root mean square error.

4.2.3. Test-retest dataset

For the sake of clarity, only the results for eyes-closed task-free data are presented in this section, with those for eyes-open presented in the Supplementary Material.

The power spectra obtained from the first and second recording of the same session are presented in Figure 12 (top panel). The global resemblance is presented in Figure 12 (bottom panel), where the average power of each frequency band obtained by sEEGnal for all first recordings are plotted against the ones obtained for all second recordings in an X-Y plot.

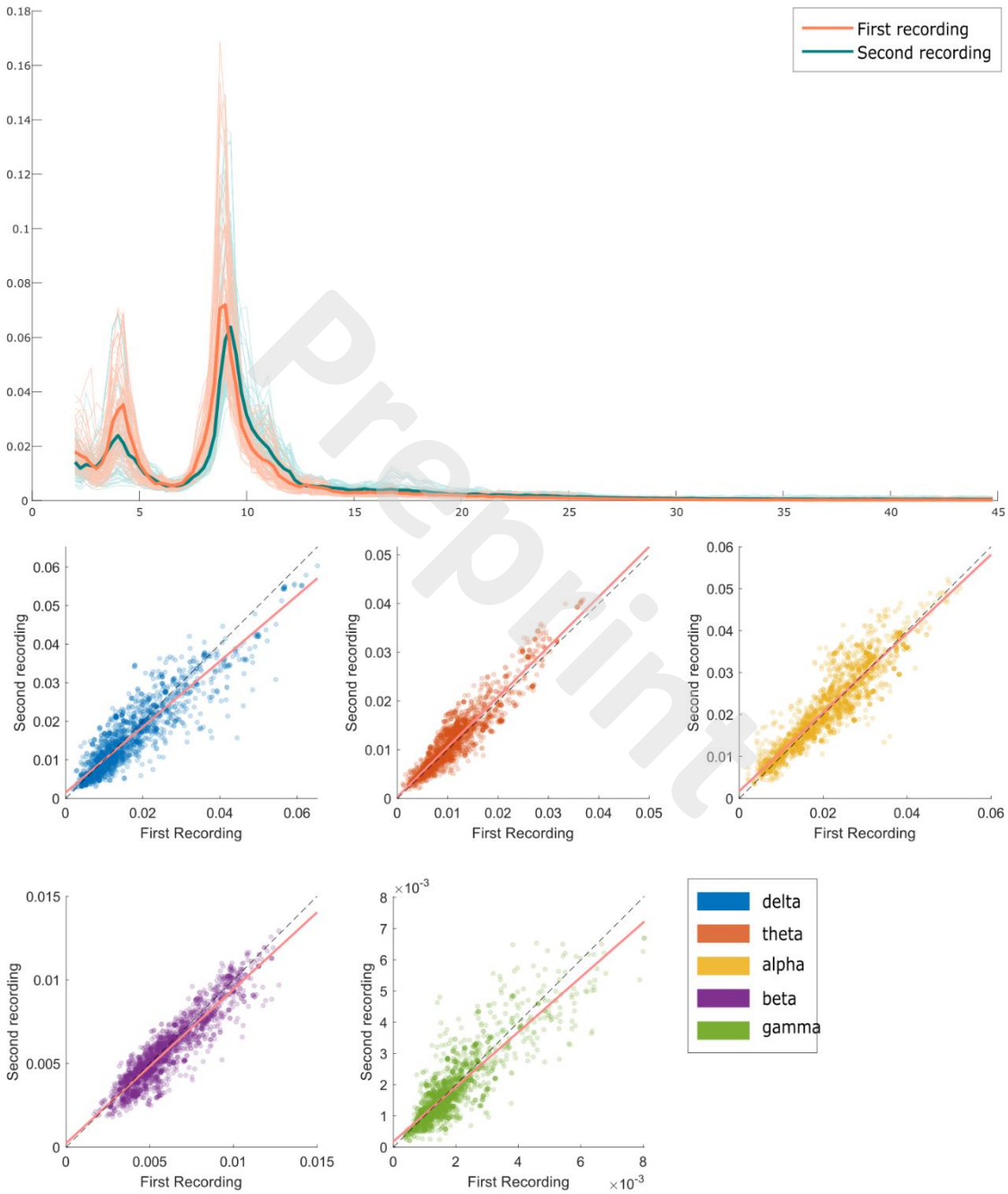

Figure 12. Comparison of power spectra obtained by sEEGnal on the test-retest dataset. On the top panel, the power spectra of both recordings. The pale lines represent individual channels, and the solid lines represent the average power spectrum across channels. On the bottom panel, an X-Y plot of the value obtained

by sEEGnal on both recordings for the power in each band. The dash line represents a perfect correspondence (1:1), and the pink line represents the least-squares line.

Regarding the results per frequency band, the NRMSE values for all channels in all recordings analysed are below 0.045, meaning the maximum difference across all the data analysed is below 4,5% of the metric range, with alpha band being the one with largest differences. (Figure 13, top panel). Regarding the spatial distribution of the differences, all channels present NRMSE values below 0,011 (1,1% of the range of the metric) (Figure 13, bottom panel), with the occipital channels in alpha band presenting the largest differences.

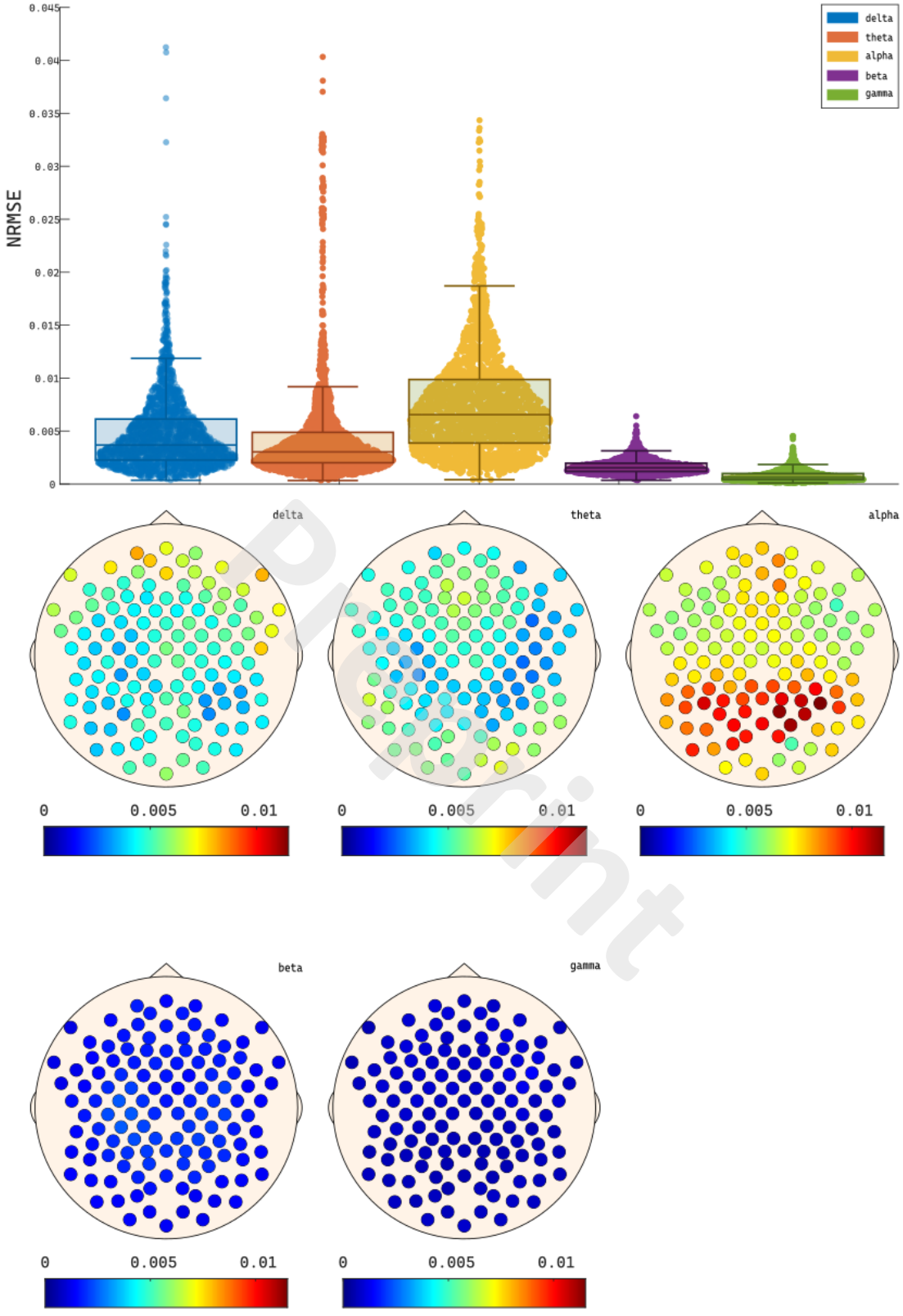

Figure 13. NRMSE values of the power spectra in the test-retest dataset. On the top panel, violin plots representing of the NRMSE distributions for all channels for each frequency band. On the bottom panels, spatial distribution of NRMSE values

across the head for each frequency band. Abbreviations: NRMSE, normalised root mean square error.

4.3. Functional Connectivity

4.3.1. LEMON dataset

The PLV obtained by sEEGnal showed a great resemblance to the ones averaged from the EEG experts (Figure 14). The global resemblance is presented as the PLV of each frequency band obtained by sEEGnal for all subjects and channels against the ones obtained by the EEG experts.

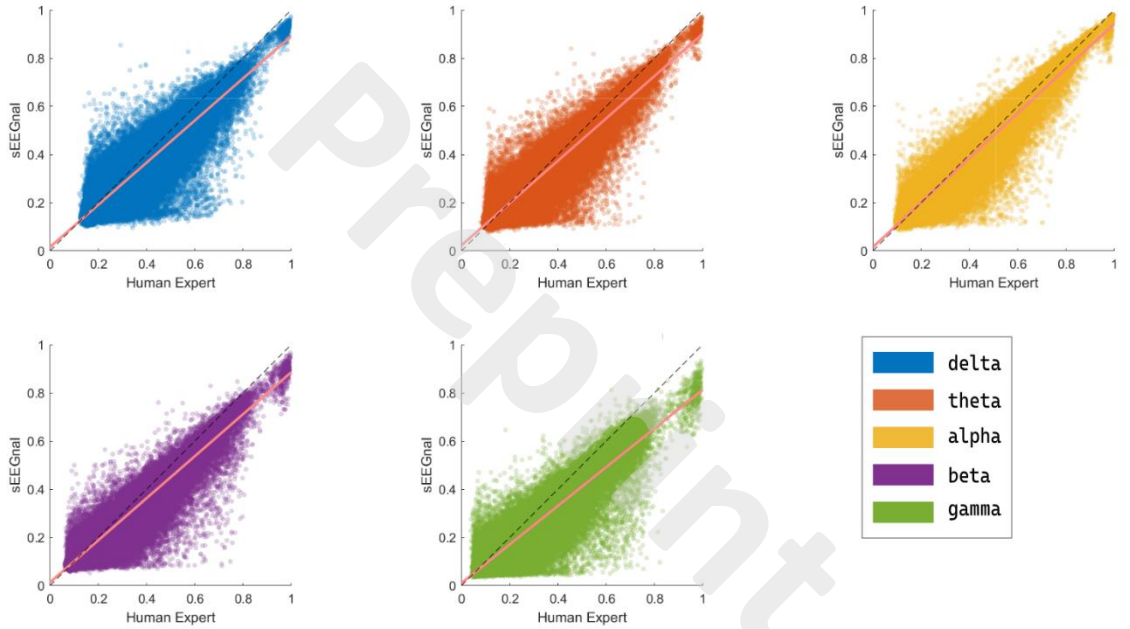

Figure 14. Comparison of PLV values obtained by the EEG experts and by sEEGnal in the LEMON dataset. An X-Y plot of the PLV values obtained in each band. The dash line represents a perfect correspondence (1:1), and the pink line represents the least-squares line.

Regarding the results per frequency band, the NRMSE values for all channels in all recordings analysed are below 0.17, meaning the maximum difference across all the data analysed is below 17% of the metric range, with gamma band being the one with more differences. (Figure 15, top). Regarding the spatial distribution of the differences, all channels present NRMSE values below 5% of the range of the metric (Figure 15, bottom panel), with the frontal channels presenting the highest differences, especially in the gamma band.

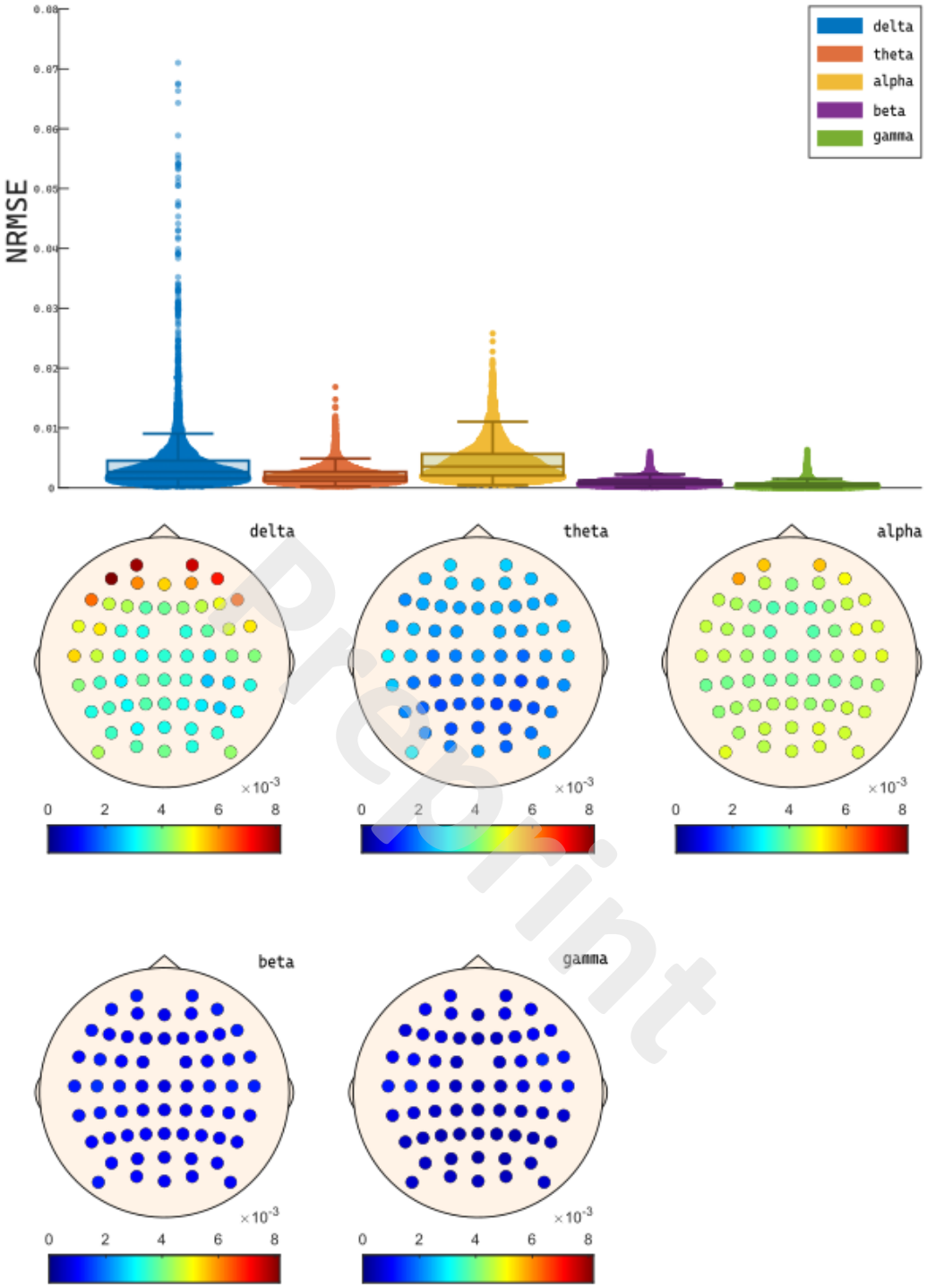

Figure 15 . NRMSE values of PLV in the LEMON dataset. On the top panel, violin plots representing of the NRMSE distributions for all channels for each frequency band. On the bottom panels, spatial distribution of NRMSE values across the head for each frequency band. Abbreviations: NRMSE, normalised root mean square error.

4.3.2. AI-Mind dataset

The PLV obtained by sEEGnal showed a great resemblance to the ones averaged from the EEG experts (Figure 16). The global resemblance is presented as the PLV of each frequency band obtained by sEEGnal for all subjects and channels against the ones obtained by the EEG experts.

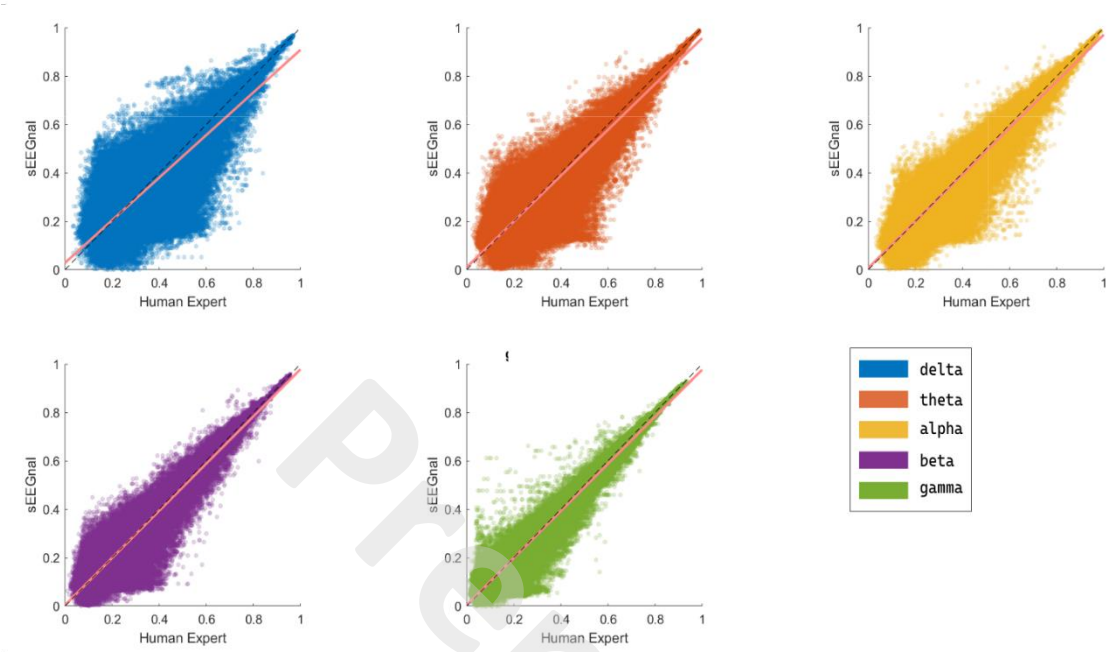

Figure 16. Comparison of PLV values obtained by the EEG experts and by sEEGnal in the AI-Mind dataset. An X-Y plot of the PLV values obtained in each band. The dash line represents a perfect correspondence (1:1), and the pink line represents the least-squares line. Abbreviations: PLV, phase locking value.

Regarding the frequency bands, the NRMSE values for all channels in all recordings analysed are below 0.12, meaning the maximum difference across all the data analysed is below 12% of the metric range, with the delta band being the one with largest differences. (Figure 17, top). Regarding the spatial distribution of the differences, all channels present NRMSE values below 3,5% of the range of the metric (Figure 17, bottom panel), with the frontal channels presenting the highest differences, especially in the delta band.

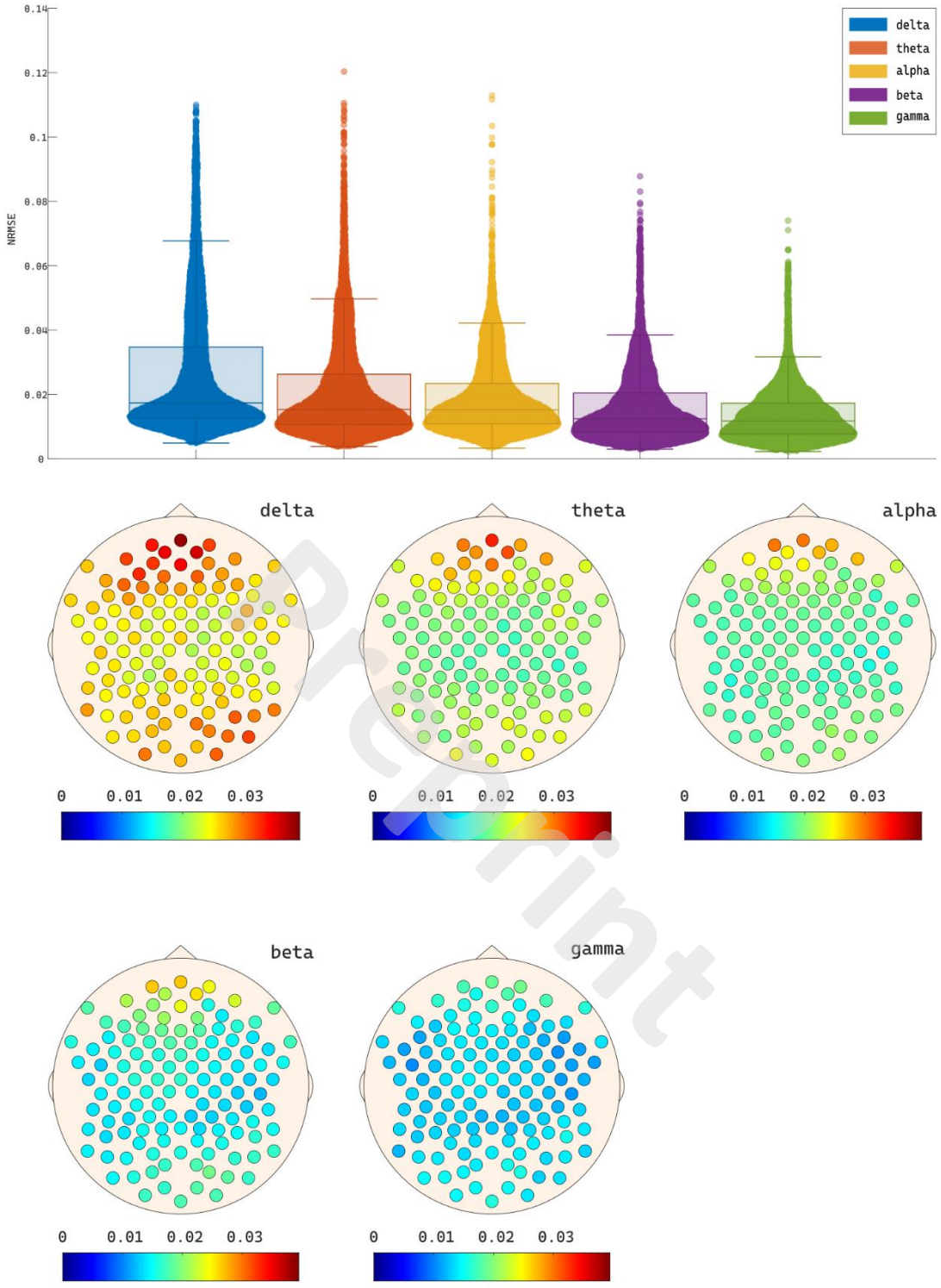

Figure 17 . NRMSE values of PLV in the AI-Mind dataset. On the top panel, violin plots representing of the NRMSE distributions for all channels for each frequency band. On the bottom panels, spatial distribution of NRMSE values across the head for each frequency band. Abbreviations: NRMSE, normalised root mean square error.

4.3.3. Test-retest dataset

For the sake of clarity, only the results for the eyes-closed task-free data are presented in this section, with those for eyes-open presented in the Supplementary Material.

The comparison of the PLV values obtained from the first and second recording of the same session are presented in Figure 18. The global resemblance is presented as the PLV of each frequency band obtained by sEEGnal for all subjects and channels comparing the first recording and second recording on the same session in an X-Y plot.

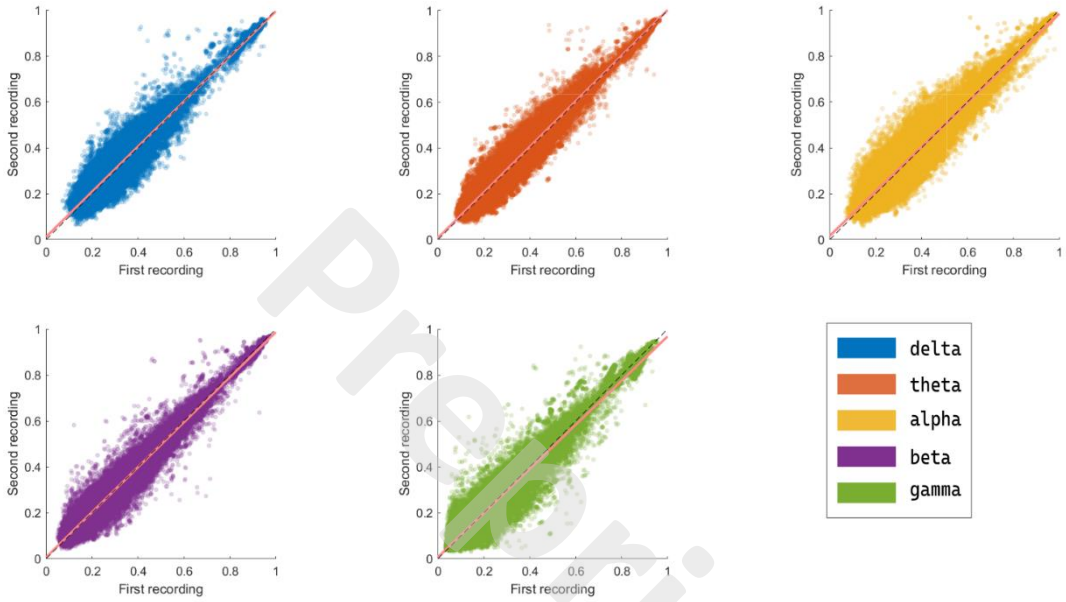

Figure 18. Comparison of PLV values obtained by sEEGnal on two recordings on the same session. An X-Y plot of the values obtained by sEEGnal for both recordings. The dash line represents a perfect correspondence (1:1), and the pink line represents the least-squares line.

Regarding the results per frequency band, the NRMSE values for all channels in all recordings analysed are below 0.09, meaning the maximum difference across all the data analysed is below 9% of the metric range, with the alpha band being the one with largest differences. (Figure 19, top). Regarding the spatial distribution of the differences, all channels present NRMSE values below 3% of the range of the signal (Figure 19, bottom panel), with the frontal channels presenting the largest differences in the alpha band, followed by frontal and occipital channels presenting large differences in the gamma band

.

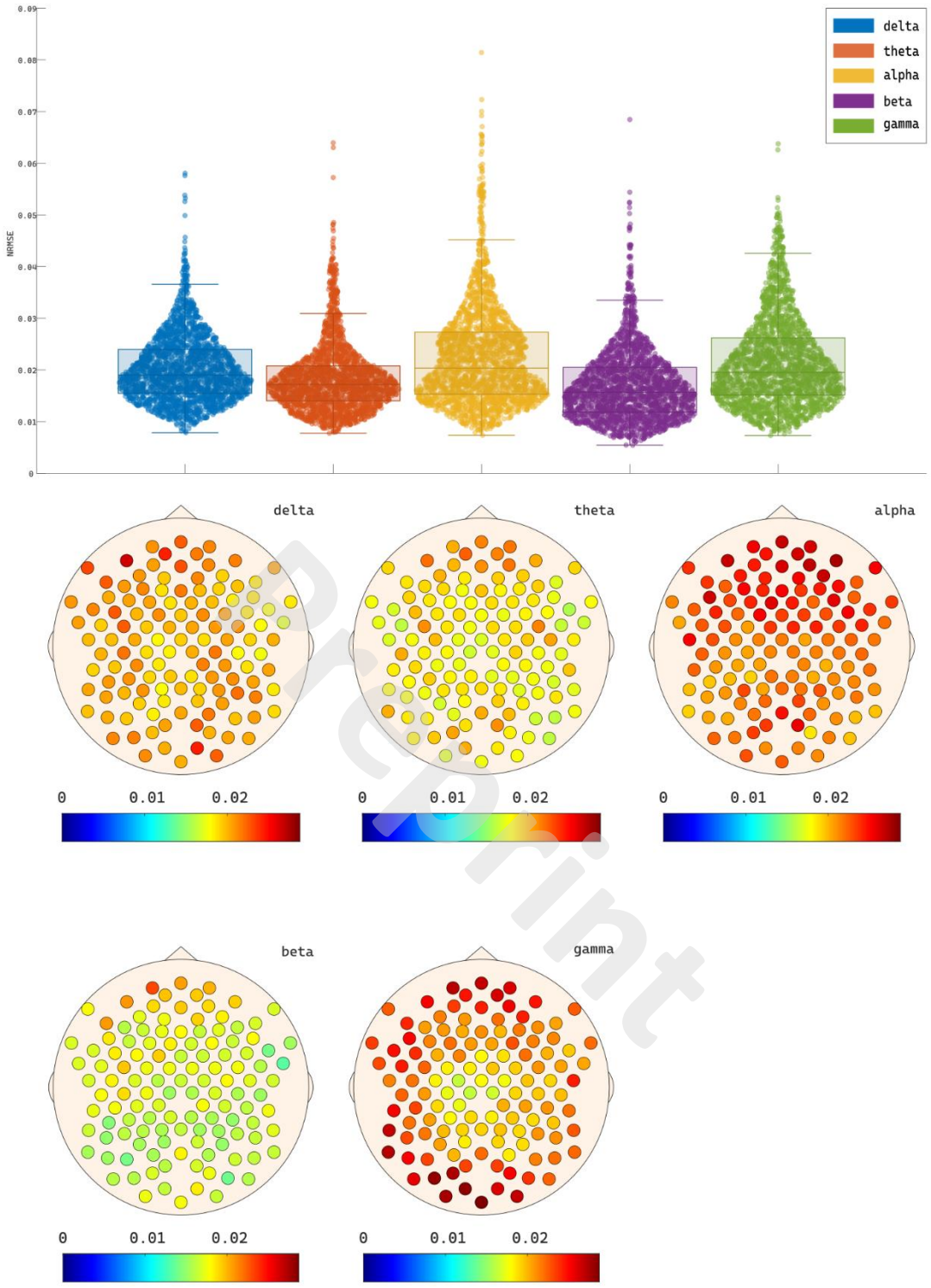

Figure 19. NRMSE values of PLV in the test-retest dataset. On the top panel, violin plots representing of the NRMSE distributions for all channels for each frequency band. On the bottom panels, spatial distribution of NRMSE values across the head for each frequency band. Abbreviations: NRMSE, normalised root mean square error.

5. Discussion

In this work, we present sEEGnal, an automatic and comprehensive pipeline for EEG pre-processing. The pipeline is designed as a modular and scalable framework for automatic EEG preprocessing. sEEGnal comprises three high-level modules (standardisation, bad channel detection, and artefact detection) that follow widely accepted guidelines for EEG pre-processing. sEEGnal has been designed oriented to five vital characteristics for this type of algorithm: i) being a comprehensive EEG pre-processing pipeline; ii) being fully automatic, i.e. users without programming background can use it; iii) being, from a performance point of view, comparable to expert-driven preprocessing; iv) being time- and memory-efficient for working in large datasets; and v) being open-source. Importantly, the pipeline is evaluated against expert-driven preprocessing and in terms of preservation of downstream neurophysiological measures.

The first module, standardisation, was designed following the BIDS standard[23]. This decision aligns with two of the abovementioned characteristics (comprehensiveness and open-source) since BIDS is nowadays the current standard protocol to share large EEG datasets. Moreover, this design facilitates interoperability and reproducibility across multi-centre studies and heterogeneous datasets. The bad channel and artefact detection modules rely on the classification of independent components by means of ICLabel[11]. The bad channel criteria assess the key features of bad channels, namely high impedance, impossible amplitudes (both high and low amplitudes), abnormal power spectrum, gel bridges, and amplitudes deviating from amplitude variance ranges. The artefacts are classified into the common types of artefacts, namely eye-related, muscle-related, sensor-related, and “other”. Since artefact detection is also based on IC classification, the pipeline was specifically designed to detect muscle- and sensor-related artefacts first, which could otherwise dominate the ICs and result in the ocular and “other” artefacts being missed.

For this work, we aimed to evaluate the performance of sEEGnal, benchmarked against the performance of EEG experts when pre-processing real EEG recordings. To this end, we evaluated sEEGnal performance based on the bad channel and artefact detection metadata, neurophysiological measurements commonly used in EEG experiments, and

the time and memory required to pre-process the recordings. This multi-level evaluation framework allows performance to be interpreted not only in terms of preprocessing decisions but also in terms of preservation of downstream neurophysiological properties.

Regarding the metadata, the results showed that its performance can be compared to that of EEG experts. The first results did not demonstrate any significant differences in the number of bad channels, and the spatial distributions of the most common bad channels were similar, in which fronto-temporal channels dominated. Neither did the number of artefacts significantly differ between sEEGnal and EEG experts, although the classification of the artefacts did: sEEGnal identified proportionally more eye- and muscle-related artefacts, whereas EEG experts showed a higher proportion of electronic jumps and artefacts classified as “other”. When assessing the number of rejected components, both sEEGnal and EEG experts rejected a comparable number of components. These results demonstrate that sEEGnal captured the essence of bad quality data, identifying correctly bad channels, artefacts, and independent components. This achievement is vital prior to compare the neurophysiological outcomes derived from the data pre-processed by sEEGnal and EEG experts.

To draw better conclusions, not only the metadata should be analysed. In this study, we estimated and analysed two common features used in neurophysiological studies, namely power spectrum and functional connectivity (by means of PLV)[24]. This approach allowed us to assess whether sEEGnal is valid for use in neuroscientific works. Regarding the power analysis, the power spectra obtained by sEEGnal resembles with high accuracy those obtained by EEG experts both in the AI-Mind and LEMON datasets. The largest difference was found in the gamma band, which is a band with a low signal-to-noise ratio, and might be affected by differences in the level of detection of high-frequency muscle-related artifacts. When analysing the spatial distribution of the differences, i.e., analysing the performance of each channel, we found an overall good agreement, finding the largest differences over the frontal channels in the delta band. Since both eyes-open and eyes-closed task-free recordings were analysed together, this difference may be related to differences in the identification of eye-related artefacts and/or components. Nevertheless, we observed that the differences’ magnitude is low compared to the range of the feature (around 8%).

For functional connectivity, we found overall good agreement, but with higher deviations than in the power spectrum analysis. This was expected when considering the nature of both neurophysiological measures; the power spectrum being one of the most robust measures (and so it is reflected in the results), and functional connectivity far more dependent on the pre-processing decisions[25,26]. Regarding the resemblance, i.e., comparing the absolute PLV values, the PLV values obtained after applying sEEGnal are consistently lower in all frequency bands, especially in the delta and gamma band. When analysing the results by sensors, frontal channels were the ones with largest differences. Again, this difference may be related to eye-related artefacts and/or components not correctly identified, which would affect PLV to a greater extent than spectral power.

Another key feature to analyse is the consistency of the neurophysiological metrics obtained after applying sEEGnal[27–29]. For that end, we selected different recordings from the same session of each subject. It was expected that recordings from the same subject recorded withing a 10-minute period would present similar neurophysiological outcomes. For power analysis, the results showed an overall good consistency, with the largest differences in frontal channels in delta band for open-eyes and in occipital channels in alpha band for closed-eyes. These differences were expected due to the nature of power spectrum, with eye movements affecting the delta band[30] and with very large differences between eyes-open and eyes-closed conditions in the alpha band[31].

Regarding the time required to pre-process a single EEG recording, there were no significant differences in the average time required to complete each module between sEEGnal and EEG experts. In contrast, when estimating the standard deviation of the time used for a single EEG recording, the EEG experts presented a much higher variability, indicating poorer consistency than sEEGnal. In addition, sEEGnal did not present problems associated with humans, like tiredness or available working hours. The results and the nature of the algorithm make sEEGnal a robust solution for pre-processing large EEG datasets.

Importantly, this open-source algorithm has been tested in two different datasets, one public and one private, using two different manufacture's device and different configurations (such as the number of channels, the sample frequency, or the length of

the recordings). These results highlight the potential of sEEGnal to generalize across different hardware setups and acquisition protocols.

Although the results in this work demonstrate that the outcomes of sEEGnal are overall comparable to those of human expert pipelines, three limitations merit discussion. Firstly, for this work we had access to only two datasets, limiting the validation of sEEGnal in a wider variety of EEG manufacturers. Nevertheless, the two datasets used in this study have sufficient quality to proof the validity of sEEGnal. The same applies to the reduce number of EEG experts. Secondly, the current version of sEEGnal heavily relies on the use of external packages, especially ICLabel[11], with the intrinsic risk of depending on external packages. Nevertheless, ICLabel is a widely used tool, and uses machine learning algorithms trained by millions of EEG recordings labelled by expert all around the world. It would unfeasible, and extremely inefficient, to try and replicate this effort independently for sEEGnal. Finally, sEEGnal has been only tested in resting-state data. An evaluation of sEEGnal in task-related EEG experiment would strengthen the proof-of-concept of sEEGnal.

In conclusion, sEEGnal represents a robust, fully automatic, and comprehensive pipeline for EEG pre-processing that achieves performance comparable to that of expert EEG practitioners. Its modular design, adherence to widely accepted standards, and ability to handle diverse datasets efficiently make it a versatile tool for both small- and large-scale studies. The pipeline reliably identifies bad channels, artefacts, and independent components, while preserving the integrity of key neurophysiological measures such as spectral power and functional connectivity. Moreover, sEEGnal demonstrates superior consistency and reproducibility compared to human experts, and its open-source nature ensures accessibility and adaptability for the broader neuroscience community. Collectively, these features establish sEEGnal as a valuable, state-of-the-art solution for automatic EEG pre-processing.

6. Code availability

The updated source code of sEEGnal may be found in https://github.com/FedeC3N/sEEGnal.

The sEEGnal version and all the scripts developed in this study for testing sEEGnal may be found in https://github.com/FedeC3N/sEEGnal_perfomance.

7. Funding

The author(s) declare financial support was received for the research, authorship, and/or publication of this article. This work has received funding from the European Union's Horizon 2020 research and innovation programme under grant agreement No. 964220. This paper reflects only the authors' view, and the Commission is not responsible for any use that may be made by the information it contains. C.H-H. was supported by the South-Eastern Norway Regional Health Authority (Helse Sør-Øst RHF), project number 2024019.

8. Acknowledgment

The AI-Mind dataset is stored on the *Tjenester for Sensitive Data* (TSD) facilities, owned by the University of Oslo, operated and developed by the TSD service group at the University of Oslo, IT-Department (USIT). (tsd-drift@usit.uio.no).

9. References

[1] A. Biasiucci, B. Franceschiello, M.M. Murray, Electroencephalography, Current Biology 29 (2019) R80–R85. https://doi.org/https://doi.org/10.1016/j.cub.2018.11.052.

[2] M. Teplan, FUNDAMENTALS OF EEG MEASUREMENT M . Teplan, Measurement Science Review 2 (2002).

[3] M. Boly, O. Gosseries, M. Massimini, M. Rosanova, Functional Neuroimaging Techniques, in: The Neurology of Consciousness: Cognitive Neuroscience and Neuropathology, 2015. https://doi.org/10.1016/B978-0-12-800948-2.00002-9.

[4] X. Jiang, G. Bin Bian, Z. Tian, Removal of artifacts from EEG signals: A review, Sensors (Switzerland) 19 (2019). https://doi.org/10.3390/s19050987.

[5] C. Pernet, M.I. Garrido, A. Gramfort, N. Maurits, C.M. Michel, E. Pang, R. Salmelin, J.M. Schoffelen, P.A. Valdes-Sosa, A. Puce, Issues and recommendations from the OHBM COBIDAS MEEG committee for reproducible EEG and MEG research, Nat. Neurosci. 23 (2020). https://doi.org/10.1038/s41593-020-00709-0.

[6] L. Simmatis, E.E. Russo, J. Geraci, I.E. Harmsen, N. Samuel, Technical and clinical considerations for electroencephalography-based biomarkers for major depressive disorder, Npj Mental Health Research 2 (2023). https://doi.org/10.1038/s44184-023-00038-7.

[7] C. Pernet, S. Appelhoff, G. Flandin, C. Phillips, A. Delorme, R. Oostenveld, BIDS-EEG: an extension to the Brain Imaging Data Structure (BIDS) Specification for electroencephalography, BIDS-EEG: An Extension to the Brain Imaging Data Structure (BIDS) Specification for Electroencephalography (2018).

[8] A. Gramfort, M. Luessi, E. Larson, D.A. Engemann, D. Strohmeier, C. Brodbeck, R. Goj, M. Jas, T. Brooks, L. Parkkonen, M. Hämäläinen, MEG and EEG data analysis with MNE-Python, Front. Neurosci. (2013). https://doi.org/10.3389/fnins.2013.00267.

[9] D. Liu, Q. Wang, Y. Zhang, X. Liu, J. Lu, J. Sun, A study on quality assessment of the surface EEG signal based on fuzzy comprehensive evaluation method, Computer Assisted Surgery 24 (2019). https://doi.org/10.1080/24699322.2018.1557888.

[10] D.M. Alschuler, C.E. Tenke, G.E. Bruder, J. Kayser, Identifying electrode bridging from electrical distance distributions: A survey of publicly-available EEG data using a new method, Clinical Neurophysiology 125 (2014). https://doi.org/10.1016/j.clinph.2013.08.024.

[11] L. Pion-Tonachini, K. Kreutz-Delgado, S. Makeig, ICLabel: An automated electroencephalographic independent component classifier, dataset, and website, Neuroimage 198 (2019) 181. https://doi.org/10.1016/J.NEUROIMAGE.2019.05.026.

[12] X. Jiang, G. Bin Bian, Z. Tian, Removal of artifacts from EEG signals: A review, Sensors (Switzerland) 19 (2019). https://doi.org/10.3390/s19050987.

[13] R. Oostenveld, P. Fries, E. Maris, J.M. Schoffelen, FieldTrip: Open source software for advanced analysis of MEG, EEG, and invasive electrophysiological data, Comput. Intell. Neurosci. 2011 (2011). https://doi.org/10.1155/2011/156869.

[14] A. Babayan, M. Erbey, D. Kumral, J.D. Reinelt, A.M.F. Reiter, J. Röbbig, H. Lina Schaare, M. Uhlig, A. Anwander, P.L. Bazin, A. Horstmann, L. Lampe, V. V. Nikulin, H. Okon-Singer, S. Preusser, A. Pampel, C.S. Rohr, J. Sacher, A. Thöne-Otto, S. Trapp, T. Nierhaus, D. Altmann, K. Arelin, M. Blöchl, E. Bongartz, P. Breig, E. Cesnaite, S. Chen, R. Cozatl, S. Czerwonatis, G. Dambrauskaite, M. Dreyer, J. Enders, M. Engelhardt, M.M. Fischer, N. Forschack, J. Golchert, L. Golz, C.A. Guran, S. Hedrich, N. Hentschel, D.I. Hoffmann, J.M. Huntenburg, R. Jost, A. Kosatschek, S. Kunzendorf, H. Lammers, M.E. Lauckner, K. Mahjoory, A.S. Kanaan, N. Mendes, R. Menger, E. Morino, K. Näthe, J. Neubauer, H. Noyan, S. Oligschläger, P. Panczyszyn-Trzewik, D. Poehlchen, N. Putzke, S. Roski, M.C. Schaller, A. Schieferbein, B. Schlaak, R. Schmidt, K.J. Gorgolewski, H.M. Schmidt, A. Schrimpf, S. Stasch, M. Voss, A. Wiedemann, D.S. Margulies, M. Gaebler, A. Villringer, Data descriptor: A mind-brain-body dataset of MRI, EEG, cognition, emotion, and peripheral physiology in young and old adults, Sci. Data 6 (2019). https://doi.org/10.1038/sdata.2018.308.

[15] A. Delorme, S. Makeig, EEGLAB: An open source toolbox for analysis of single-trial EEG dynamics including independent component analysis, J. Neurosci. Methods 134 (2004). https://doi.org/10.1016/j.jneumeth.2003.10.009.

[16] S. Makeig, A.J. Bell, T.P. Jung, T.J. Sejnowski, Independent Component Analysis of Electroencephalographic Data, in: NIPS 1995: Proceedings of the 8th International Conference on Neural Information Processing Systems, 1995.

[17] I.H. Haraldsen, C. Hatlestad-Hall, C. Marra, H. Renvall, F. Maestú, J. Acosta-Hernández, S. Alfonsin, V. Andersson, A. Anand, V. Ayllón, A. Babic, A. Belhadi, C. Birck, R. Bruña, N. Caraglia, C. Carrarini, E. Christensen, A. Cicchetti, S. Daugbjerg, R. Di Bidino, A. Diaz-Ponce, A. Drews, G.M. Giuffrè, J. Georges, P. Gil-Gregorio, D. Gove, T.M. Govers, H. Hallock, M. Hietanen, L. Holmen, J. Hotta, S. Kaski, R. Khadka, A.S. Kinnunen, A.M. Koivisto, S. Kulashekhar, D. Larsen, M. Liljeström, P.G. Lind, A. Marcos Dolado, S. Marshall, S. Merz, F. Miraglia, J. Montonen, V. Mäntynen, A.R.

Øksengård, J. Olazarán, T. Paajanen, J.M. Peña, L. Peña, D. lrabien Peniche, A.S. Perez, M. Radwan, F. Ramírez-Toraño, A. Rodríguez-Pedrero, T. Saarinen, M. Salas-Carrillo, R. Salmelin, S. Sousa, A. Suyuthi, M. Toft, P. Toharia, T. Tveitstøl, M. Tveter, R. Upreti, R.J. Vermeulen, F. Vecchio, A. Yazidi, P.M. Rossini, Intelligent digital tools for screening of brain connectivity and dementia risk estimation in people affected by mild cognitive impairment: the AI-Mind clinical study protocol, Front. Neurorobot. 17 (2023). https://doi.org/10.3389/fnbot.2023.1289406.

[18] R. Oostenveld, P. Praamstra, The five percent electrode system for high-resolution EEG and ERP measurements, Clinical Neurophysiology 112 (2001). https://doi.org/10.1016/S1388-2457(00)00527-7.

[19] A. Belouchrani, K. Abed-Meraim, J.F. Cardoso, E. Moulines, A blind source separation technique using second-order statistics, IEEE Transactions on Signal Processing 45 (1997) 434–444. https://doi.org/10.1109/78.554307.

[20] J.-P. Lachaux, E. Rodriguez, J. Martinerie, F.J. Varela, Measuring phase synchrony in brain signals, Hum. Brain Mapp. 8 (1999) 194–208. https://doi.org/10.1002/(SICI)1097-0193(1999)8:4<194::AID-HBM4>3.0.CO;2-C.

[21] R. Bruña, F. Maestú, E. Pereda, Phase locking value revisited: Teaching new tricks to an old dog, J. Neural Eng. 15 (2018). https://doi.org/10.1088/1741-2552/aacfe4.

[22] D.L. Schomer, F.H.L. da Silva, Niedermeyer's electroencephalography: Basic principles, clinical applications, and related fields: Sixth edition, 2012. https://doi.org/10.1111/j.1468-1331.2011.03406.x.

[23] K.J. Gorgolewski, T. Auer, V.D. Calhoun, R.C. Craddock, S. Das, E.P. Duff, G. Flandin, S.S. Ghosh, T. Glatard, Y.O. Halchenko, D.A. Handwerker, M. Hanke, D. Keator, X. Li, Z. Michael, C. Maumet, B.N. Nichols, T.E. Nichols, J. Pellman, J.B. Poline, A. Rokem, G. Schaefer, V. Sochat, W. Triplett, J.A. Turner, G. Varoquaux, R.A. Poldrack, The brain imaging data structure, a format for organizing and describing outputs of neuroimaging experiments, Scientific Data 2016 3:1 3 (2016) 1–9. https://doi.org/10.1038/sdata.2016.44.

[24] M.X. Cohen, Analyzing Neural Time Series Data: Theory and Practice, MIT Press (2014).

[25] C. Pernet, M.I. Garrido, A. Gramfort, N. Maurits, C.M. Michel, E. Pang, R. Salmelin, J.M. Schoffelen, P.A. Valdes-Sosa, A. Puce, Issues and recommendations from the OHBM COBIDAS MEEG committee for reproducible EEG and MEG research, Nat. Neurosci. 23 (2020). https://doi.org/10.1038/s41593-020-00709-0.

[26] S. Haufe, V. V. Nikulin, K.R. Müller, G. Nolte, A critical assessment of connectivity measures for EEG data: A simulation study, Neuroimage 64 (2013). https://doi.org/10.1016/j.neuroimage.2012.09.036.

[27] M.C. Salinsky, B.S. Oken, L. Morehead, Test-retest reliability in EEG frequency analysis, Electroencephalogr. Clin. Neurophysiol. 79 (1991). https://doi.org/10.1016/0013-4694(91)90203-G.

[28] C.E. Rolle, M. Narayan, W. Wu, R. Toll, N. Johnson, T. Caudle, M. Yan, D. El-Said, M. Watts, M. Eisenberg, A. Etkin, Functional connectivity using high density EEG shows competitive reliability and agreement across test/retest sessions, J. Neurosci. Methods 367 (2022). https://doi.org/10.1016/j.jneumeth.2021.109424.

[29] S. Gudmundsson, T.P. Runarsson, S. Sigurdsson, G. Eiriksdottir, K. Johnsen, Reliability of quantitative EEG features, Clinical Neurophysiology 118 (2007). https://doi.org/10.1016/j.clinph.2007.06.018.

[30] U. Amin, F.A. Nascimento, I. Karakis, D. Schomer, S.R. Benbadis, Normal variants and artifacts: Importance in EEG interpretation, Epileptic Disorders 25 (2023). https://doi.org/10.1002/epd2.20040.

[31] R.J. Barry, A.R. Clarke, S.J. Johnstone, C.A. Magee, J.A. Rushby, EEG differences between eyes-closed and eyes-open resting conditions, Clinical Neurophysiology 118 (2007). https://doi.org/10.1016/j.clinph.2007.07.028.

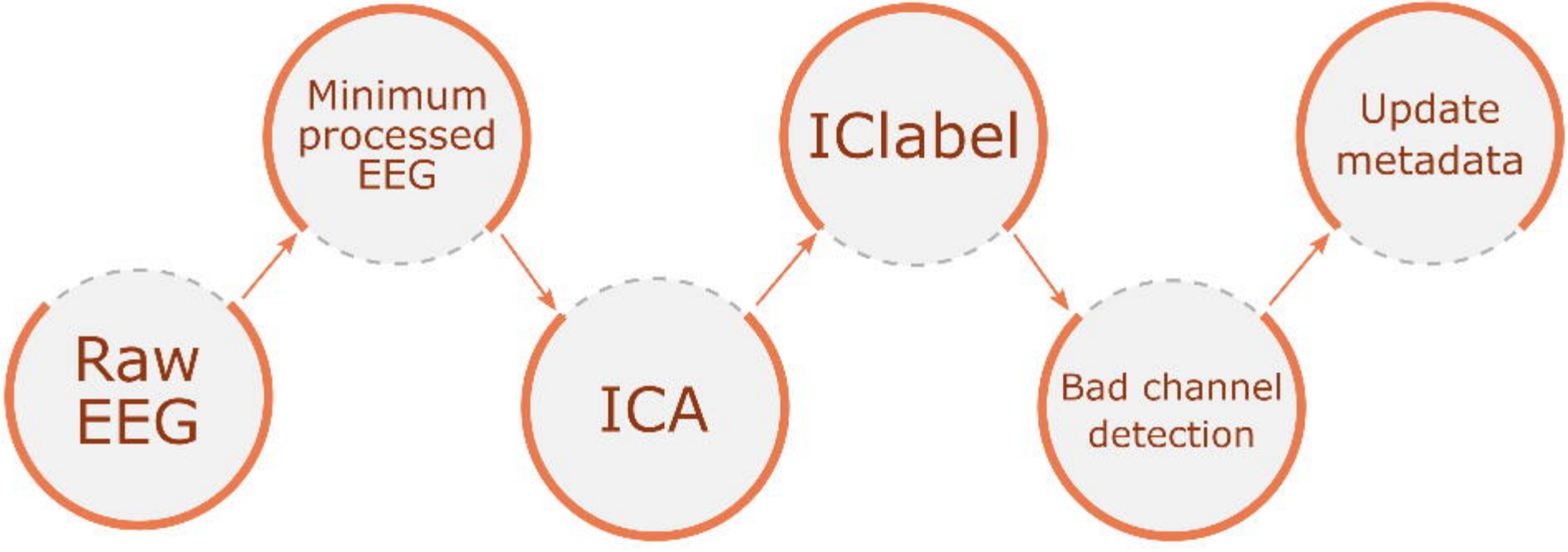
Raw EEG
Minimum processed EEG
ICA
IClabel
Bad channel detection
Update metadata

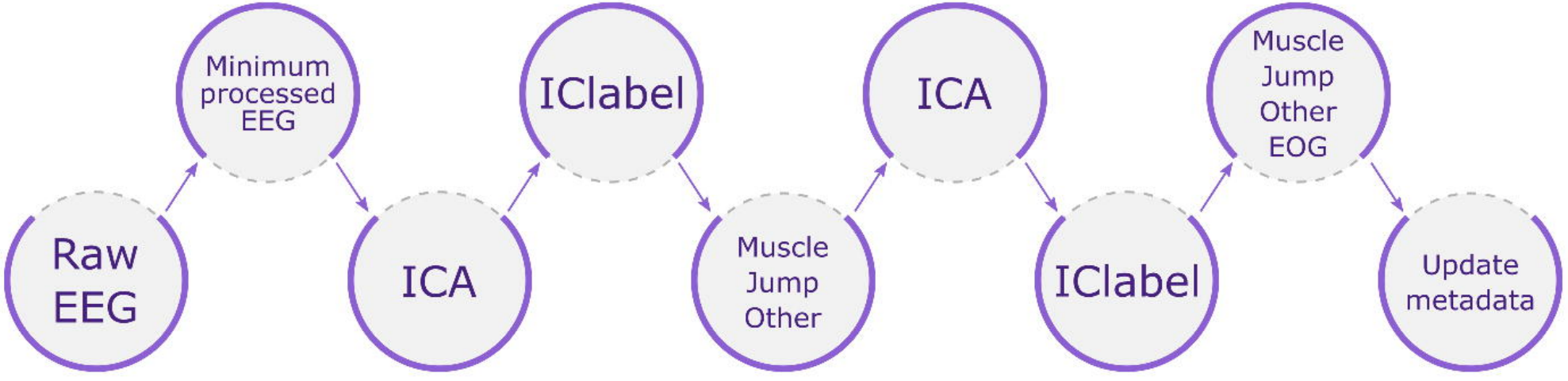
Raw EEG
Minimum processed EEG
ICA
IClabel
Muscle Jump Other
ICA
IClabel
Muscle Jump Other EOG
Update metadata

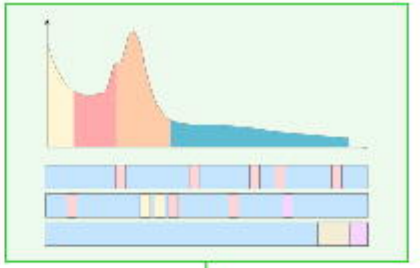

Datasets → Standardise → Pre-process → Measures → Statistics

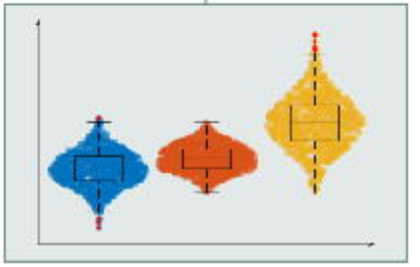

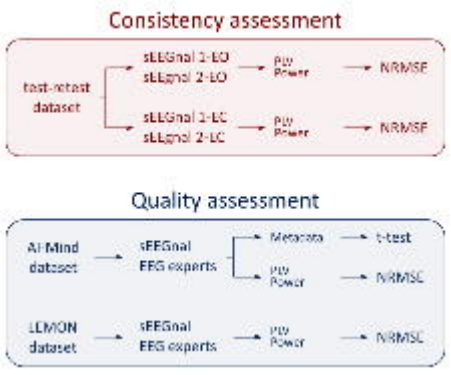
Consistency assessment
test-retest dataset
sLEGnal 1-EO
sLEGnal 2-EO
PLV Power
NRMSE
sLEGnal 1-EC
sLEGnal 2-EC
PLV Power
NRMSE
Quality assessment
Al-Mind dataset
sEEGnal EEG experts
Meacrata
t-test
PLV Power
NRMSE
LEMON dataset
sEEGnal EEG experts
PLV Power
NRMSE

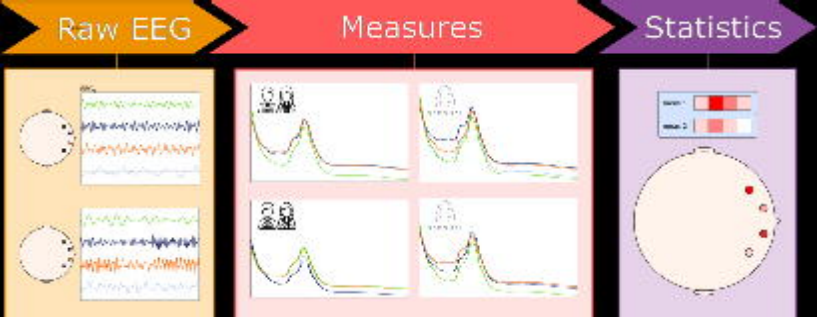
Raw EEG
Measures
Statistics

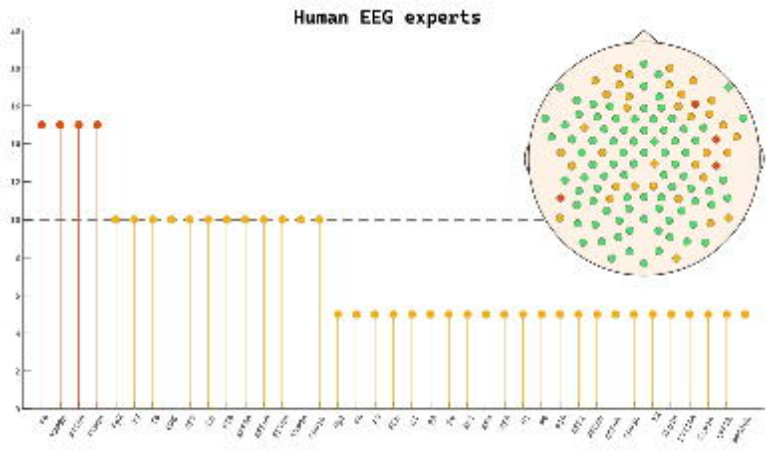
Human EEG experts

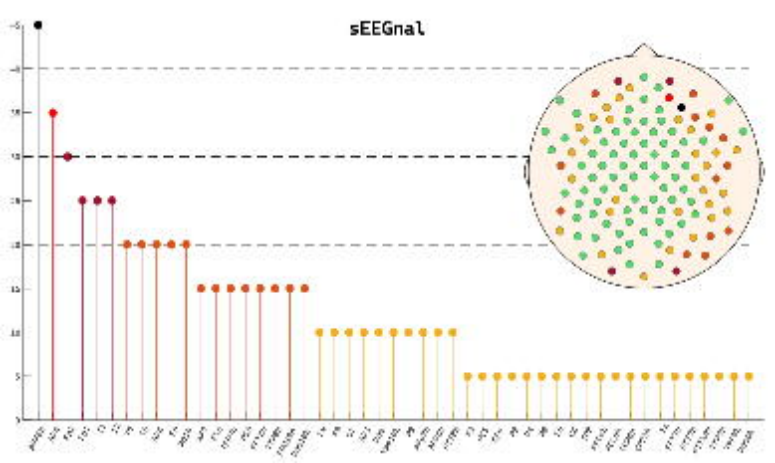
sEEGnal

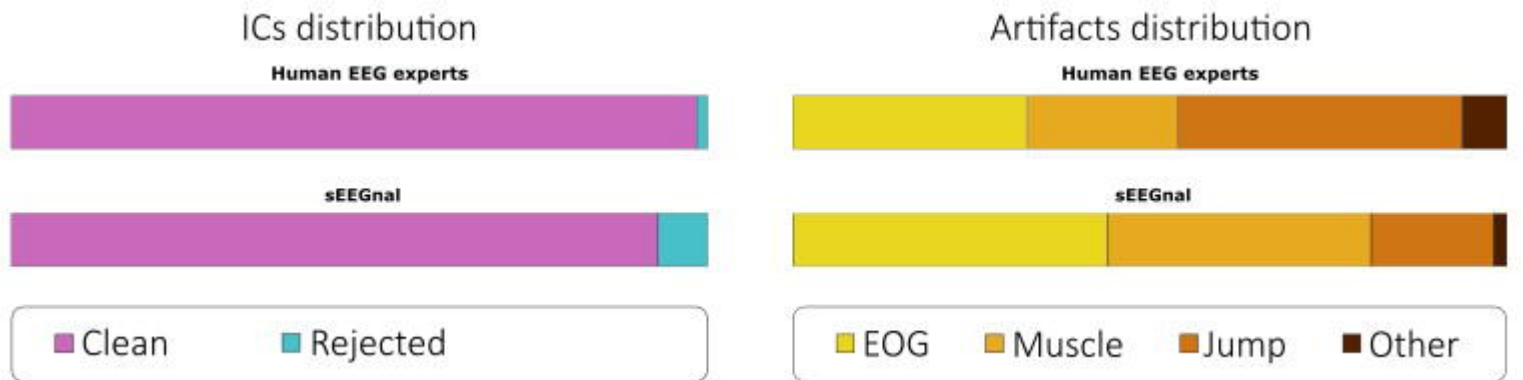
ICs distribution
Human EEG experts
sEEGnal
Clean
Rejected
Artifacts distribution
Human EEG experts
sEEGnal
EOG
Muscle
Jump
Other

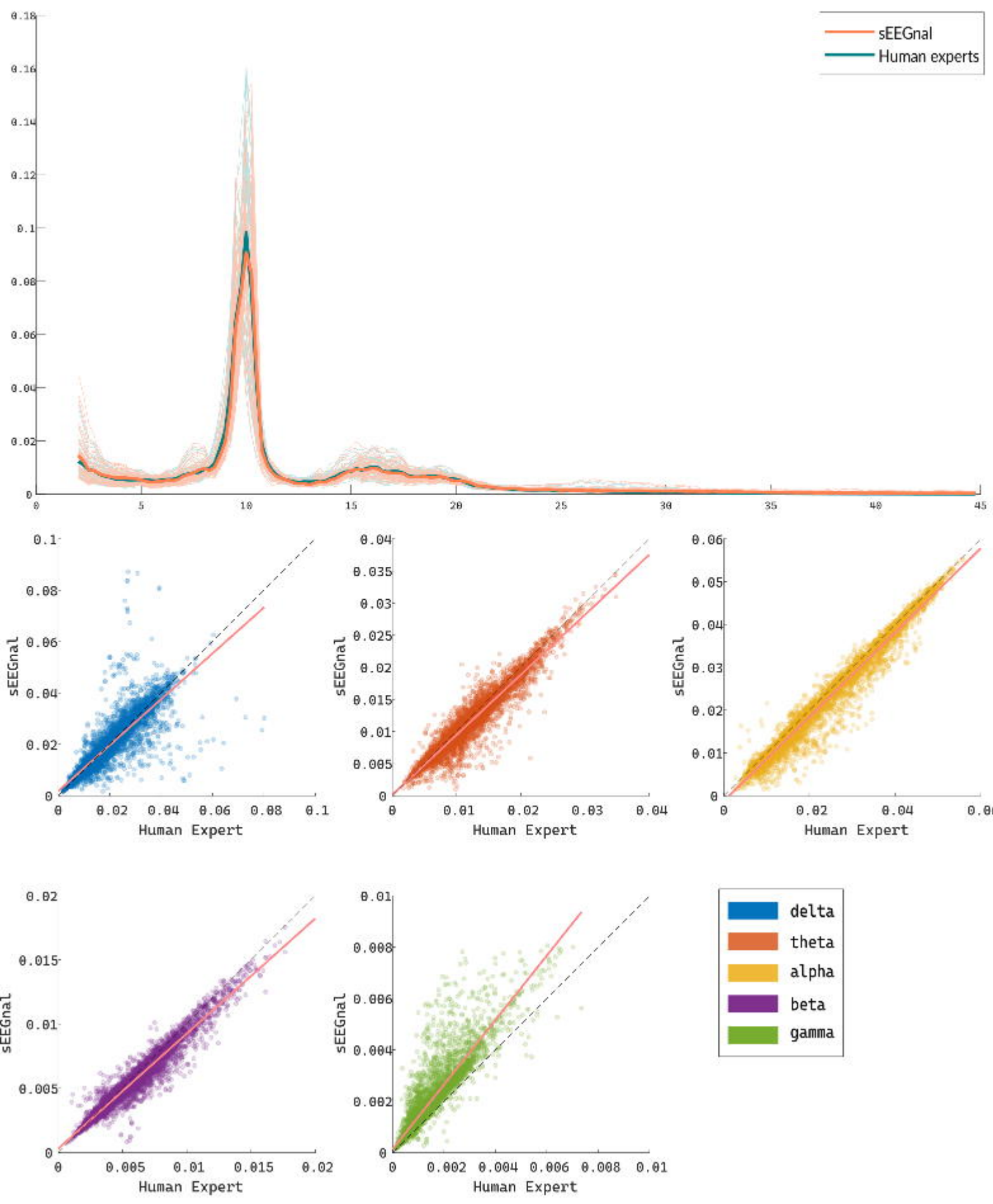
sEEGnal
Human experts
sEEGnal
Human Expert
delta
theta
alpha
beta
gamma

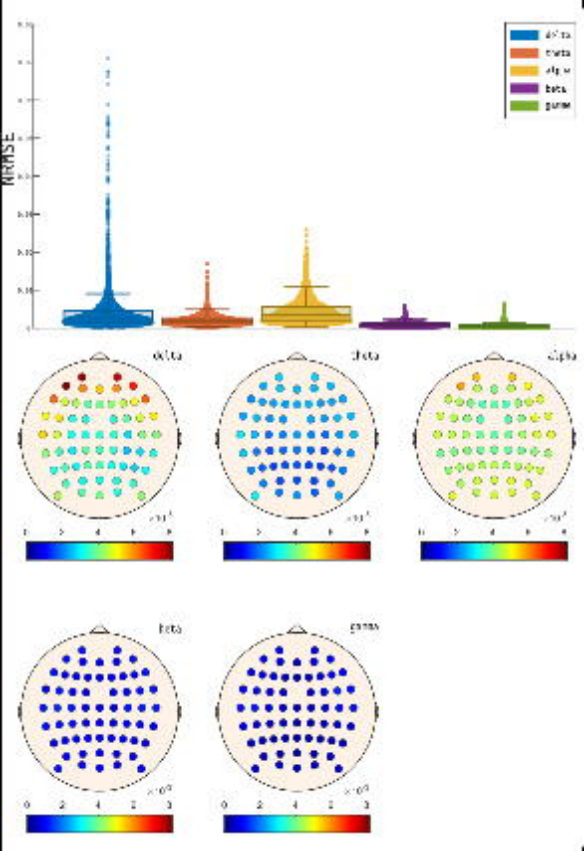
delta
theta
alpha
beta
gamma
MMSE
delta
theta
alpha
beta
gamma

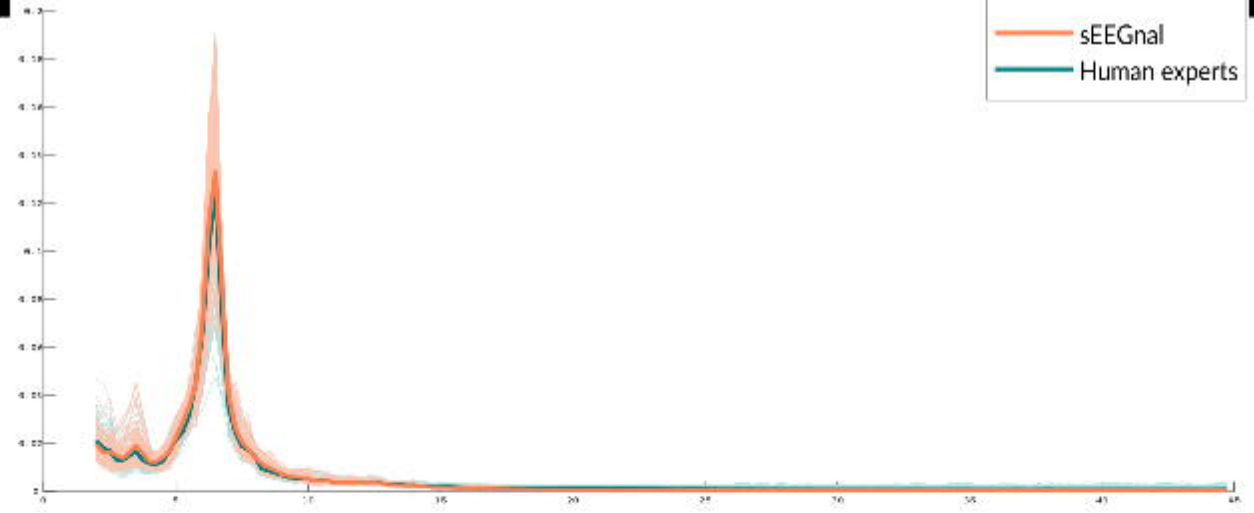
sEEGnal
Human experts

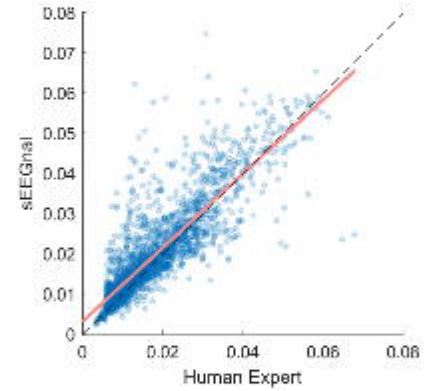
sEEGnal
Human Expert

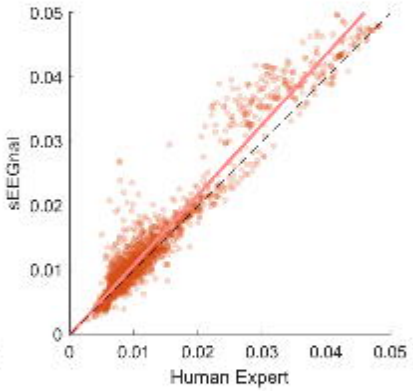
sEEGnal
Human Expert

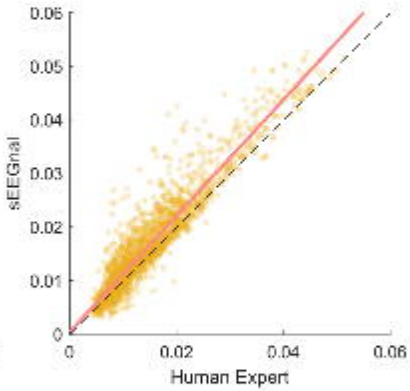
sEEGnal
Human Expert

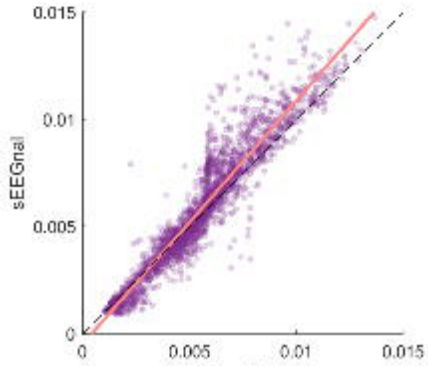
sEEGnal

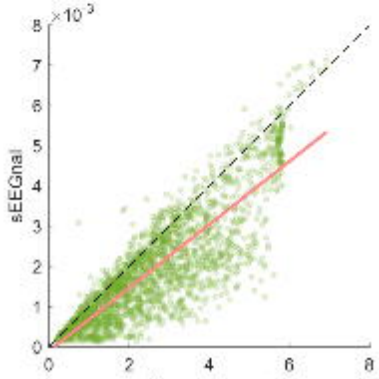
×10^-3
sEEGnal


delta
theta
alpha
beta
gamma

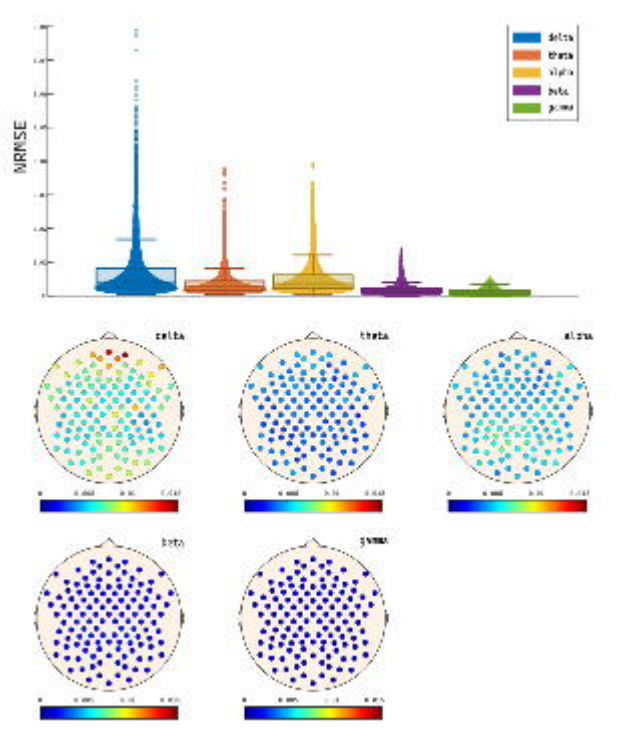
MRMSE
delta
theta
alpha
beta
gamma

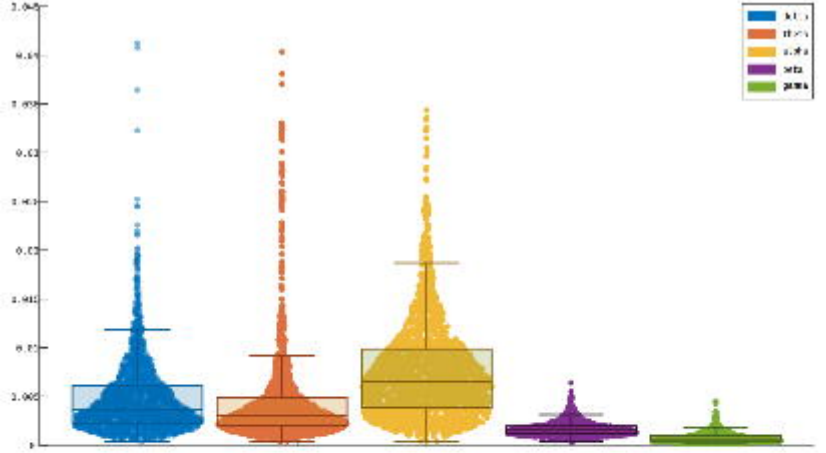

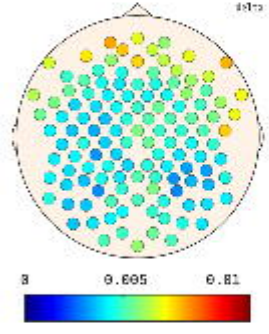
0
0.005
0.01

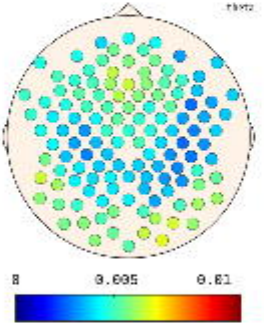
0
0.005
0.01

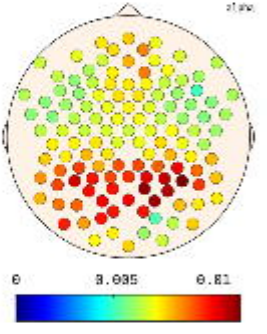
0
0.005
0.01

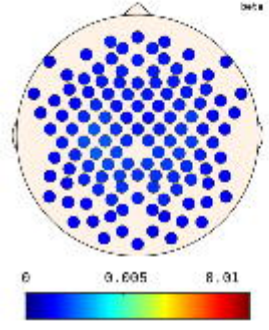
0
0.005
0.01

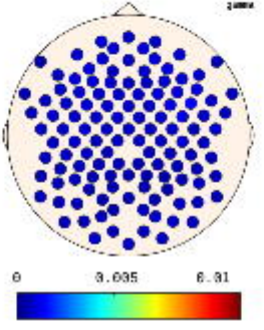
0
0.005
0.01

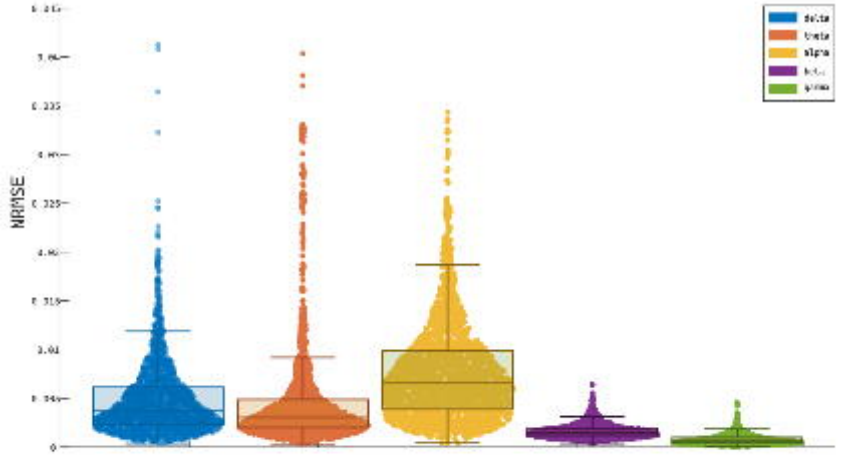
MRMSE
delta
theta
alpha

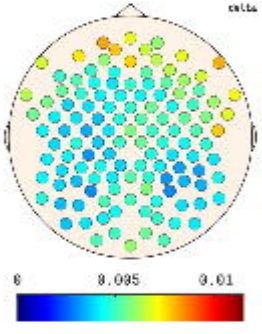
delta
0
0.005
0.01

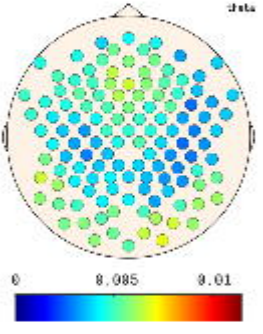
theta
0
0.005
0.01

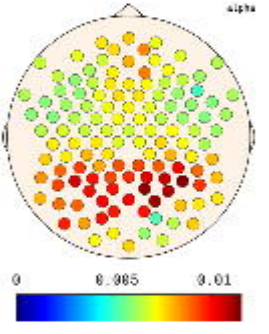
alpha
0
0.005
0.01

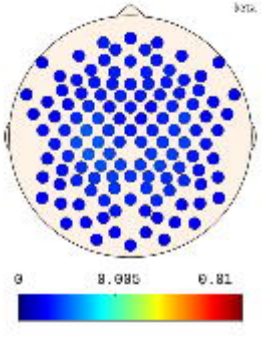
0
0.005
0.01

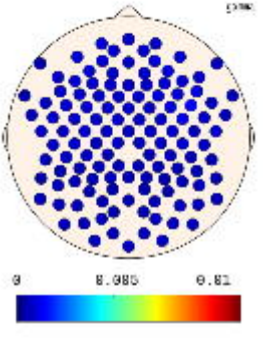
0
0.005
0.01

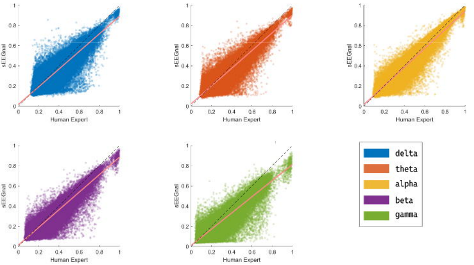

sEEGnal
Human Expert
0
0.2
0.4
0.6
0.8
1
delta
theta
alpha
beta
gamma

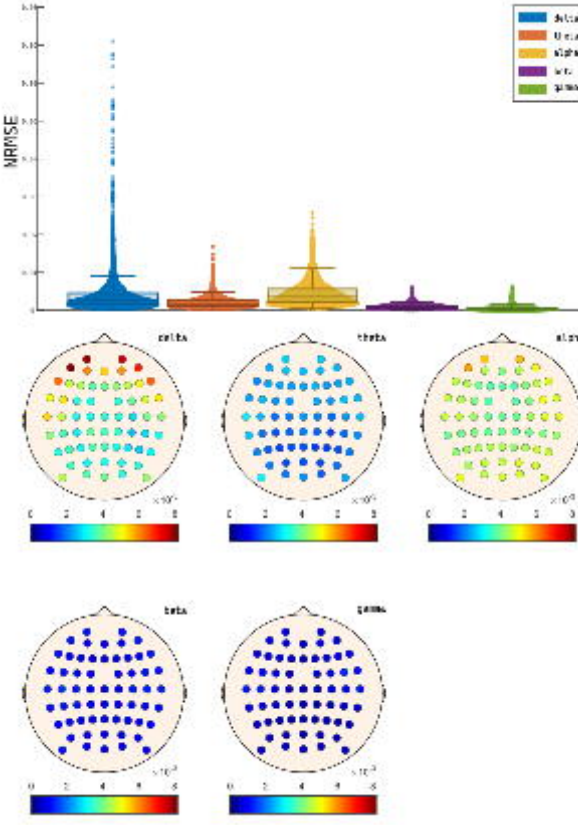
NRMSE
delta
theta
alpha
beta
gamma

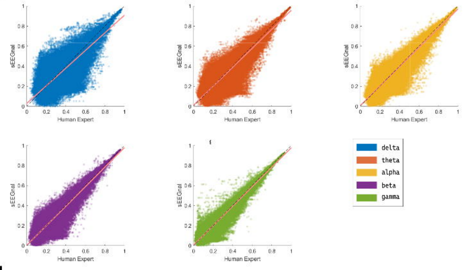
sEEGnal
Human Expert
delta
theta
alpha
beta
gamma

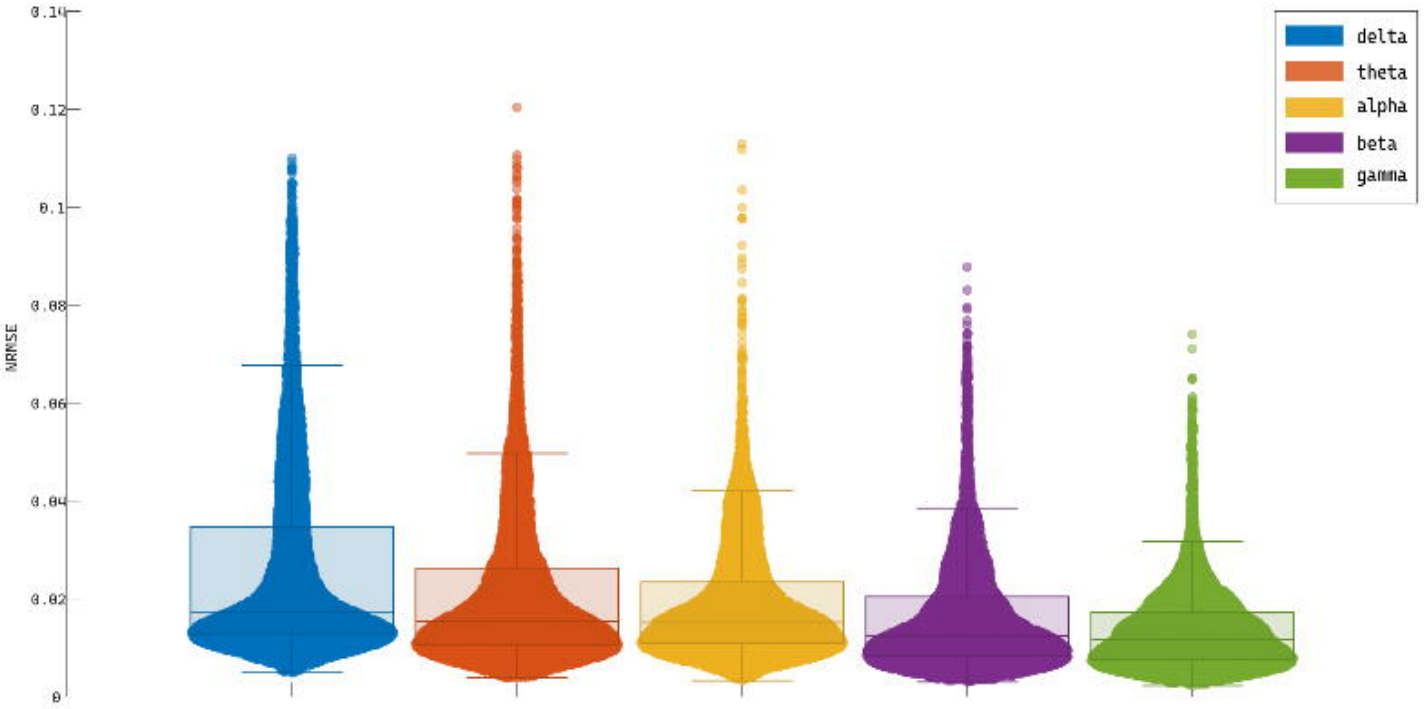
delta
theta
alpha
beta
gamma
MRMSE
0.14
0.12
0.1
0.08
0.06
0.04
0.02
0

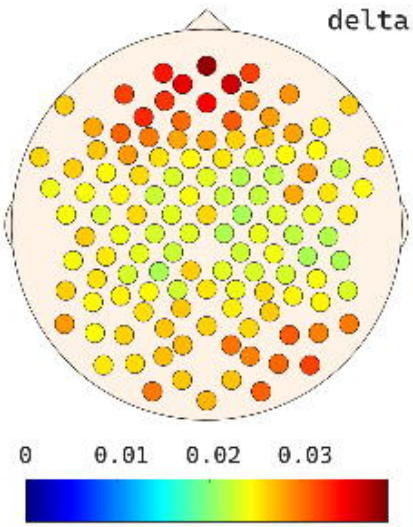
delta
0
0.01
0.02
0.03

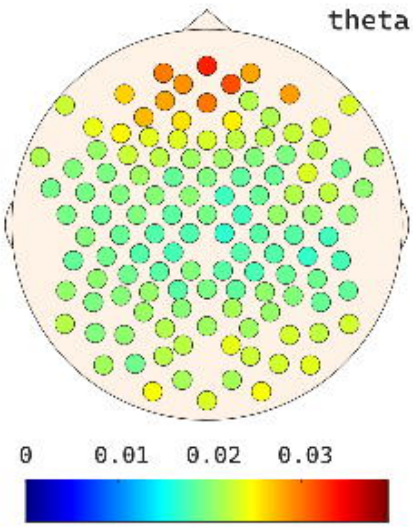
theta
0
0.01
0.02
0.03

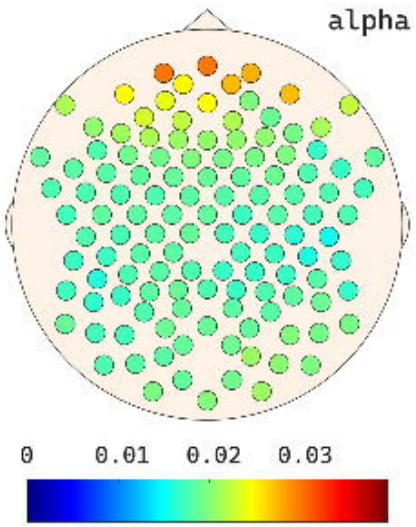
alpha
0
0.01
0.02
0.03

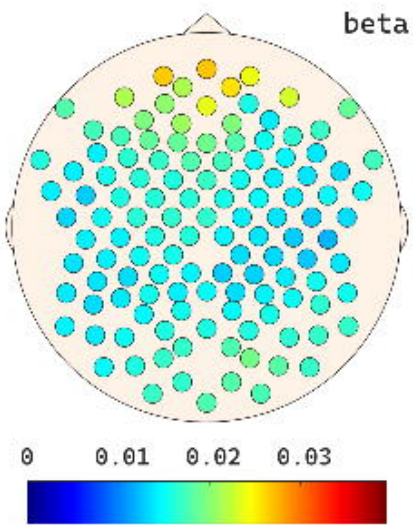
beta
0
0.01
0.02
0.03

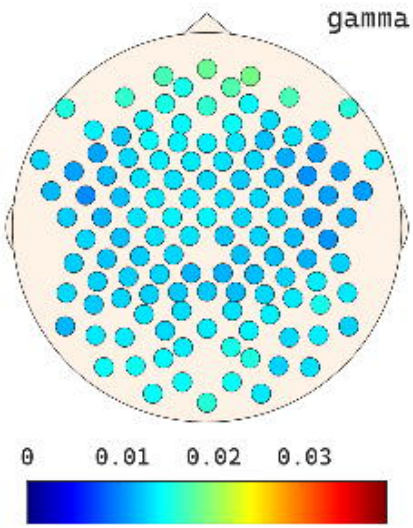
gamma
0
0.01
0.02
0.03

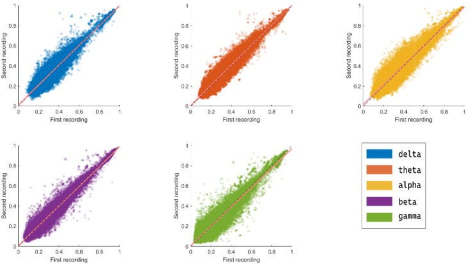

Second recording
First recording
0
0.2
0.4
0.6
0.8
1
delta
theta
alpha
beta
gamma

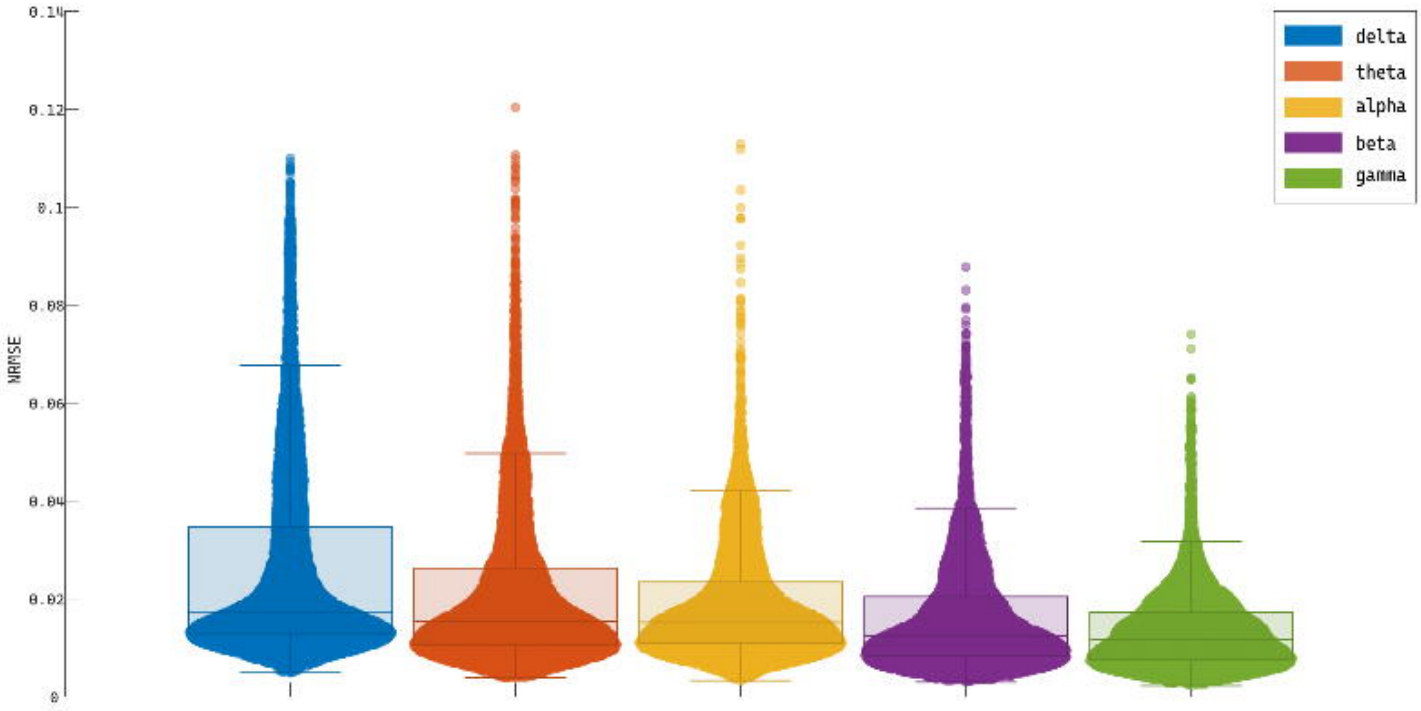
0.14
0.12
0.1
0.08
0.06
0.04
0.02
0
WRMSE
delta
theta
alpha
beta
gamma

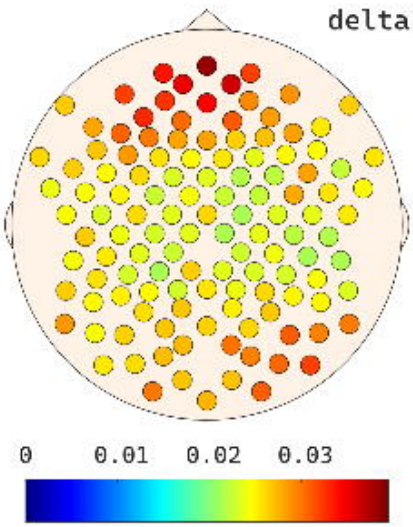
delta
0
0.01
0.02
0.03

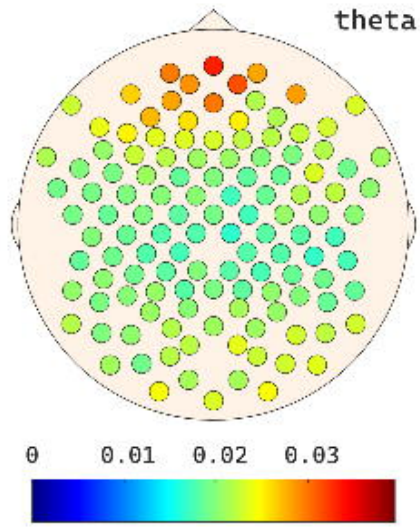
theta
0
0.01
0.02
0.03

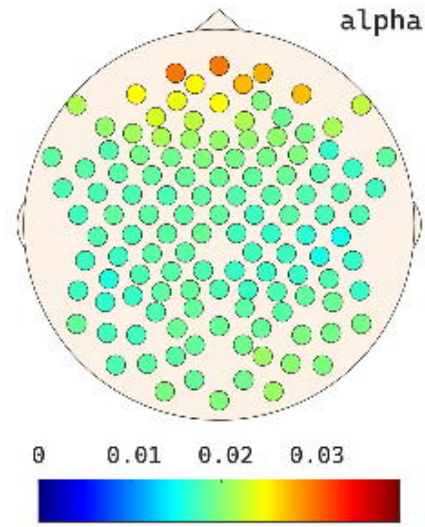
alpha
0
0.01
0.02
0.03

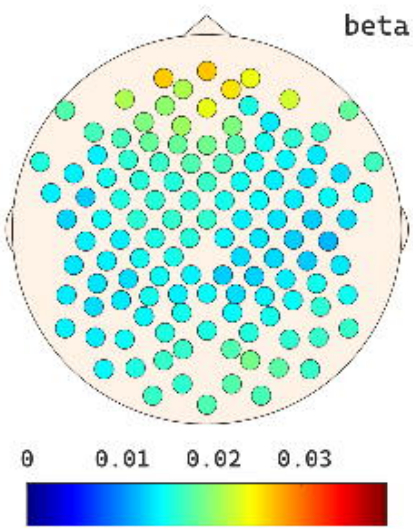
beta
0
0.01
0.02
0.03

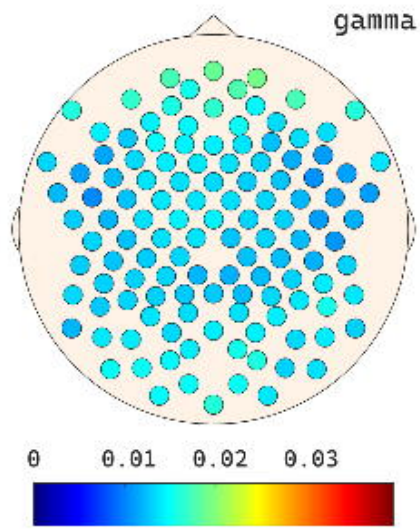
gamma
0
0.01
0.02
0.03

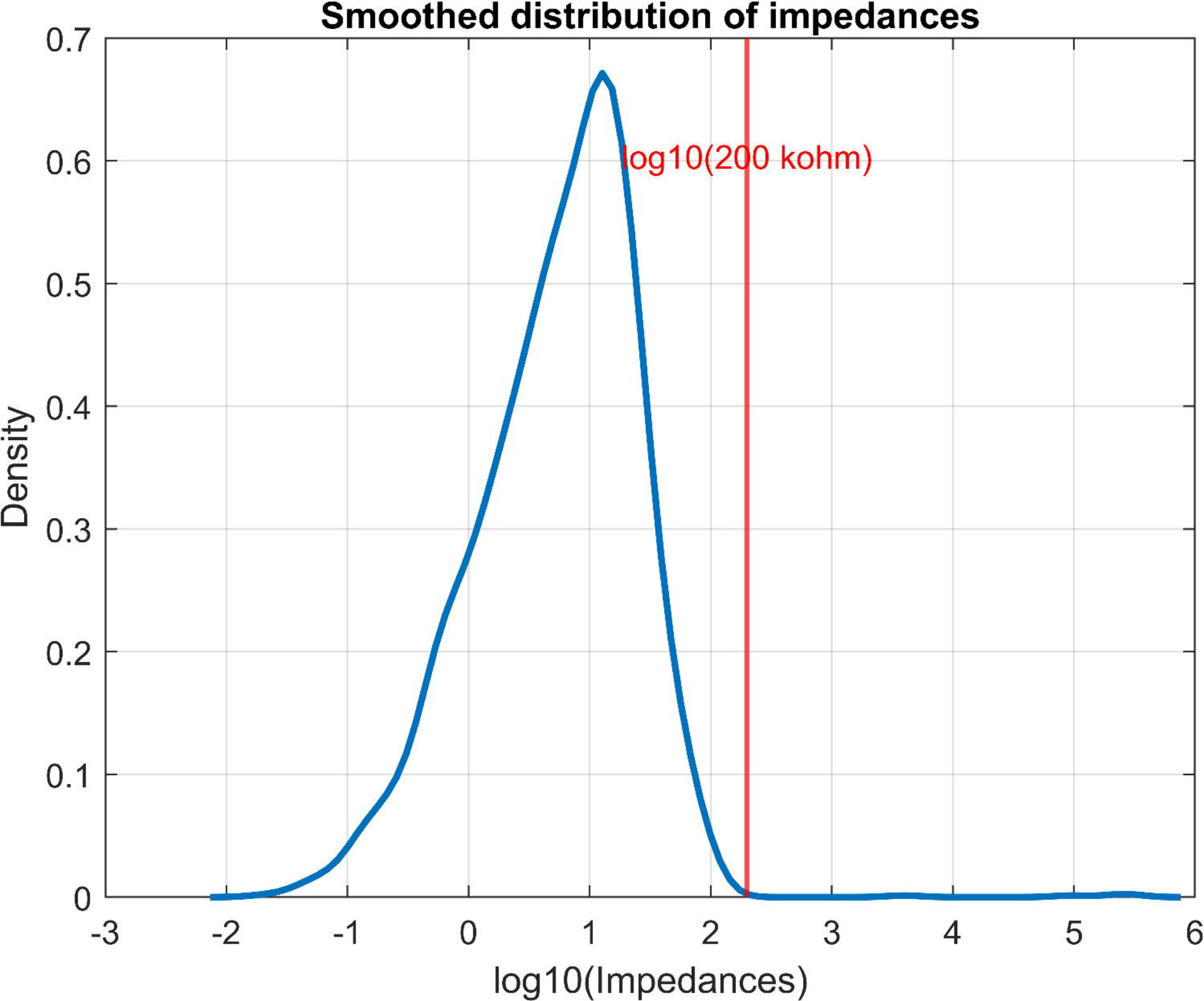
Smoothed distribution of impedances
log10(200 kohm)
Density
log10(Impedances)
0.7
0.6
0.5
0.4
0.3
0.2
0.1
0
-3
-2
-1
0
1
2
3
4
5
6

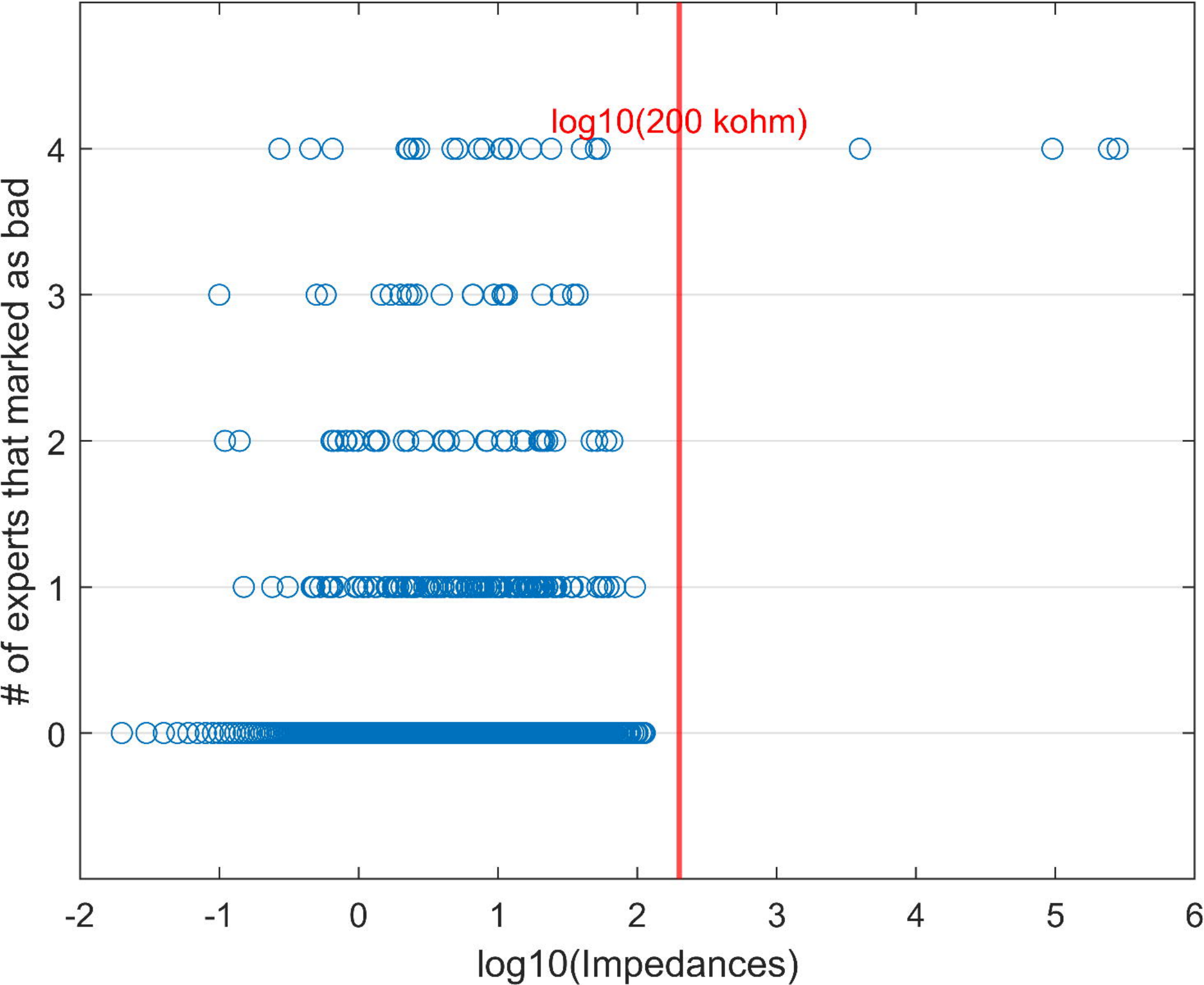
log10(200 kohm)
# of experts that marked as bad
log10(Impedances)
4
3
2
1
0
-2
-1
0
1
2
3
4
5
6

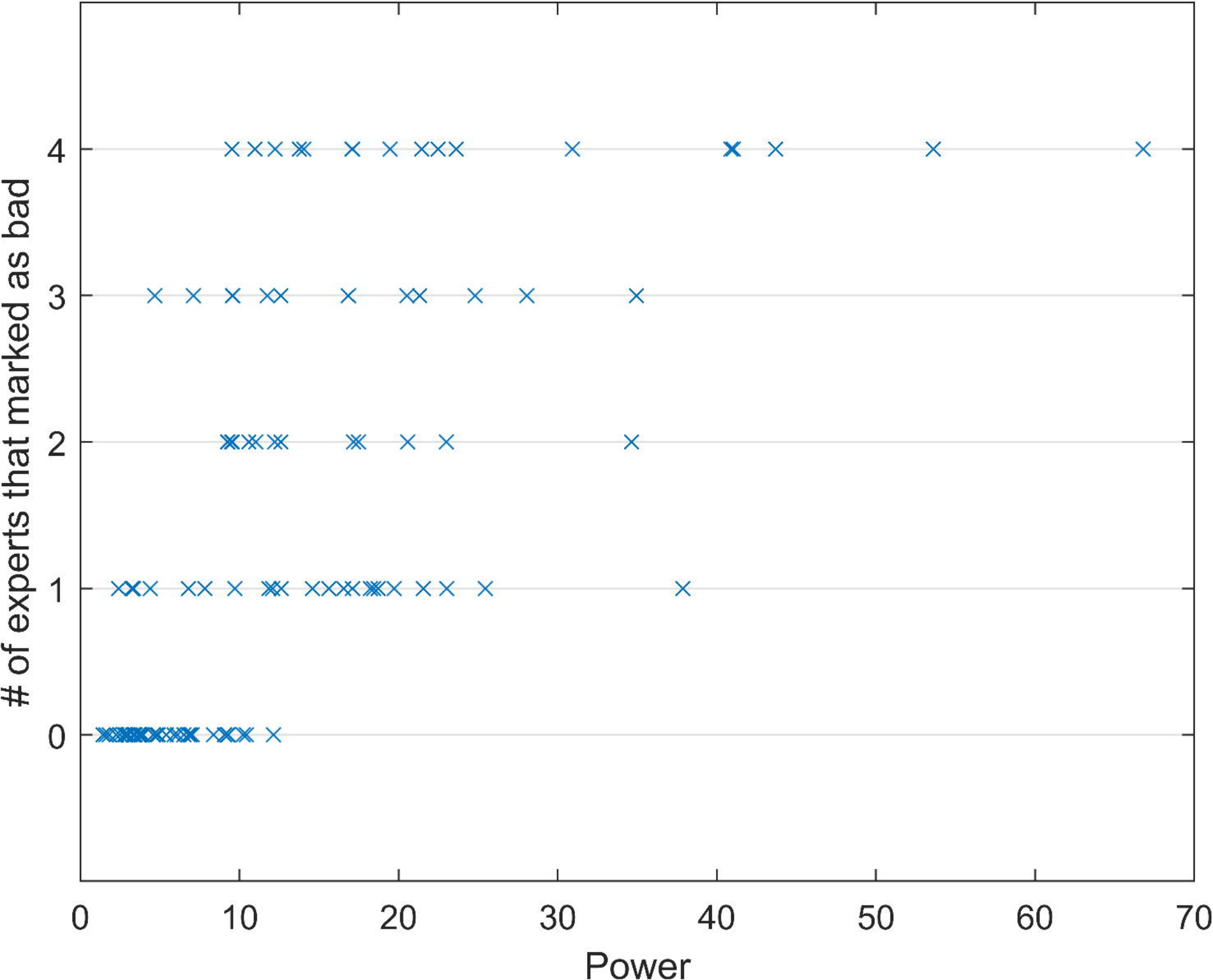
# of experts that marked as bad
4
3
2
1
0
0
10
20
30
40
50
60
70
Power

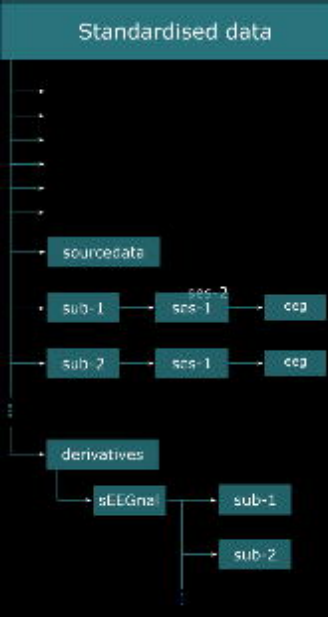
Standardised data
sourcedata
sub-1
ses-1
ses-2
eeg
sub-2
ses-1
eeg
derivatives
sEEGnal
sub-1
sub-2

```
# First, load all the measures for sEEGnal and the human EEG expert
load sEEGnal measure;
load EEG expert measure;

for each frequency band:

    select frequencies in sEEGnal measure;
    select frequencies in EEG expert measure;

    for each sensor:

        select sensor in sEEGnal measure;
        select sensor in EEG expert measure;

        for each recording:

            # Estimate correlation, and NRMSE
            NRMSE(sEEGnal measure(freq,sensor,subject),EEG expert measure(freq,sensor,subject))

        # Average across recordings for each sensor
        mean(NRMSE)

    # Plot the spatial results for each frequency band
    plot_head(NRMSE)
```

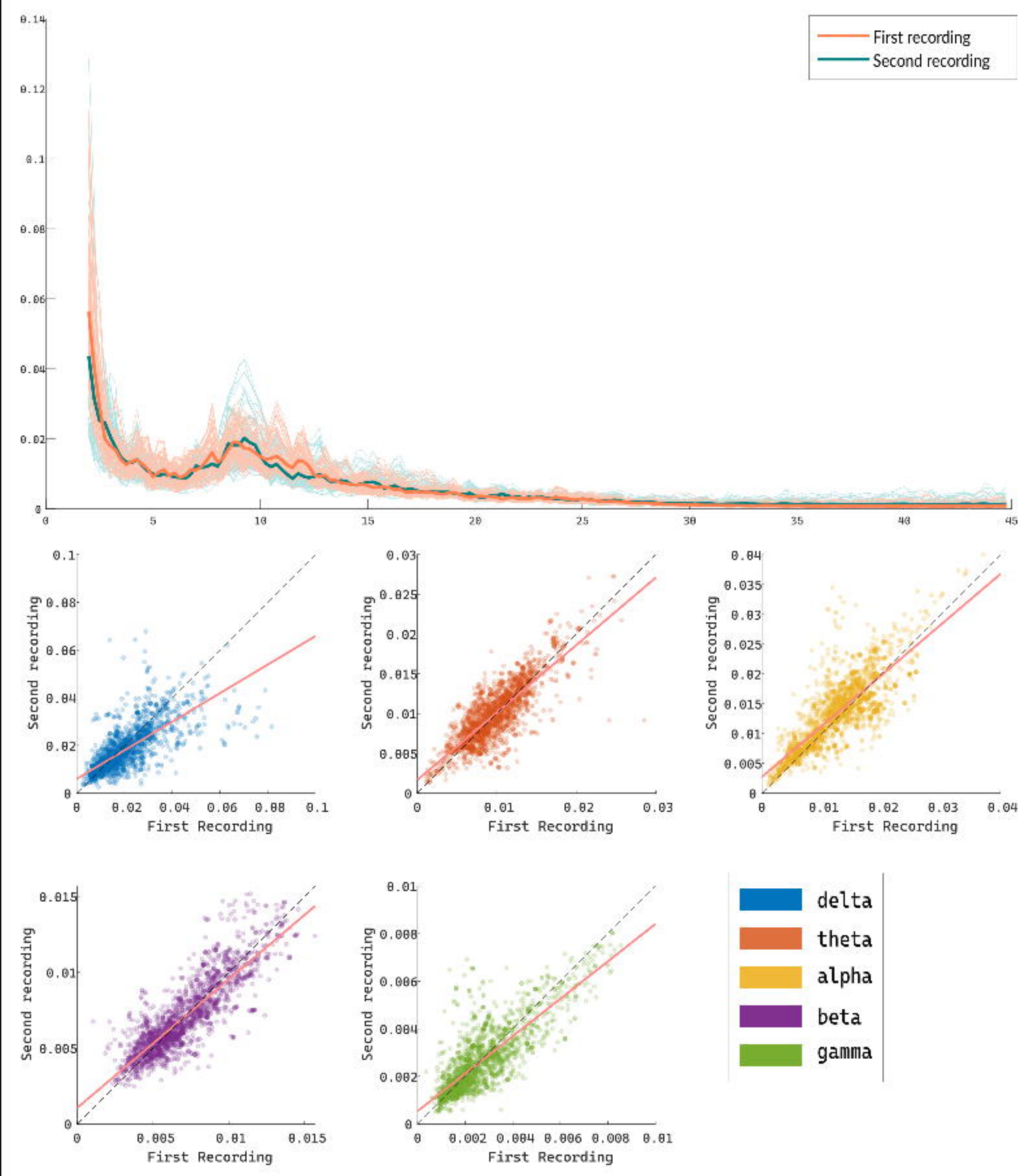
First recording
Second recording
0.14
0.12
0.1
0.08
0.06
0.04
0.02
0
0
5
10
15
20
25
30
35
40
45
Second recording
First Recording
0.1
0.08
0.06
0.04
0.02
0
0.02
0.04
0.06
0.08
0.1
0.03
0.025
0.02
0.015
0.01
0.005
0.01
0.02
0.03
0.04
0.035
0.03
0.025
0.02
0.015
0.01
0.005
0.04
0.015
0.01
0.005
0.005
0.01
0.015
0.01
0.008
0.006
0.004
0.002
0.002
0.004
0.006
0.008
0.01
delta
theta
alpha
beta
gamma

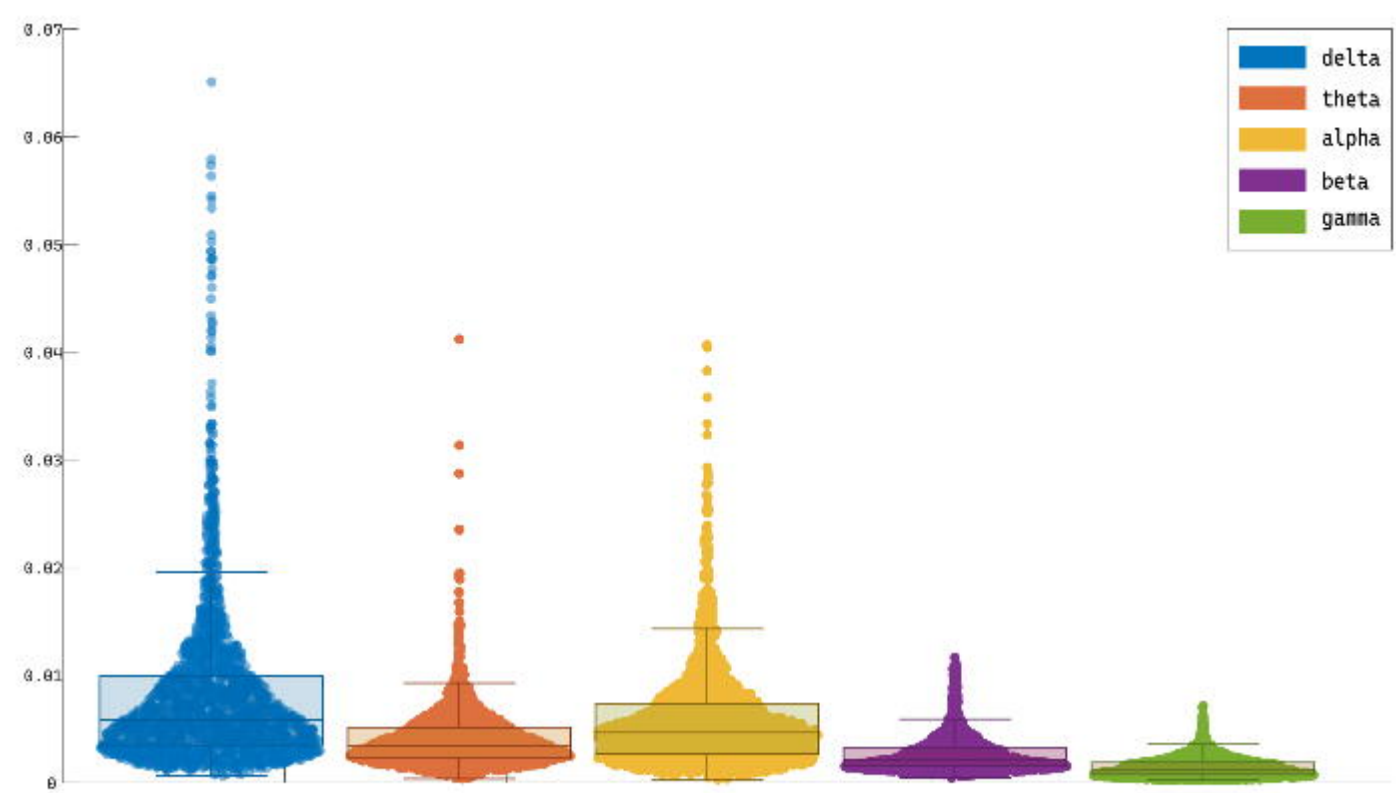
0.07
0.06
0.05
0.04
0.03
0.02
0.01
0
delta
theta
alpha
beta
gamma

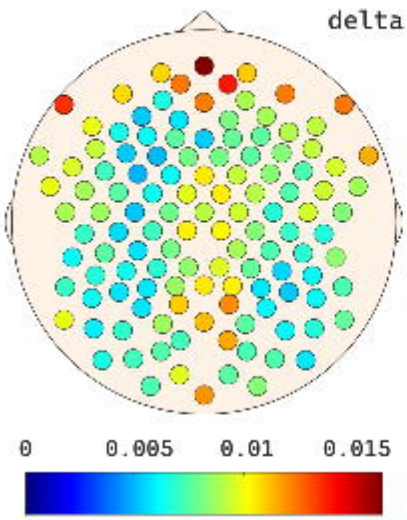
delta
0
0.005
0.01
0.015

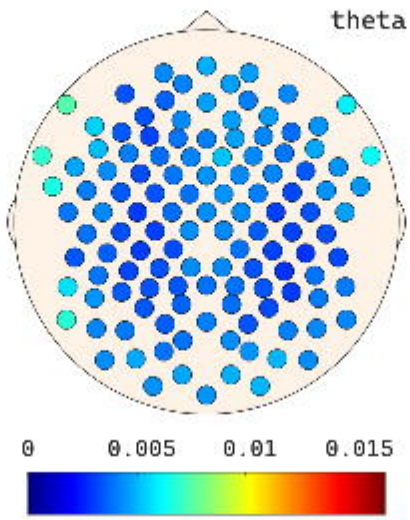
theta
0
0.005
0.01
0.015

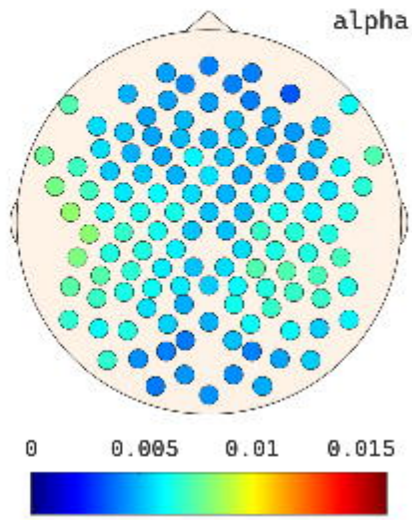
alpha
0
0.005
0.01
0.015

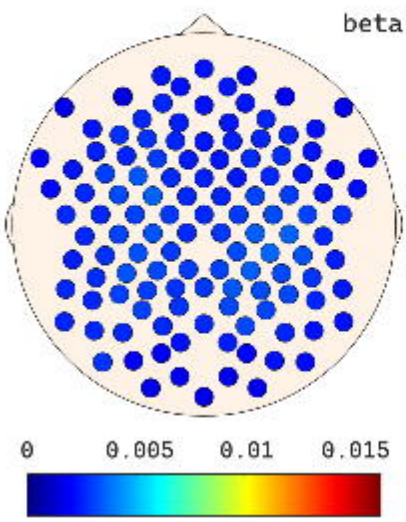
beta
0
0.005
0.01
0.015

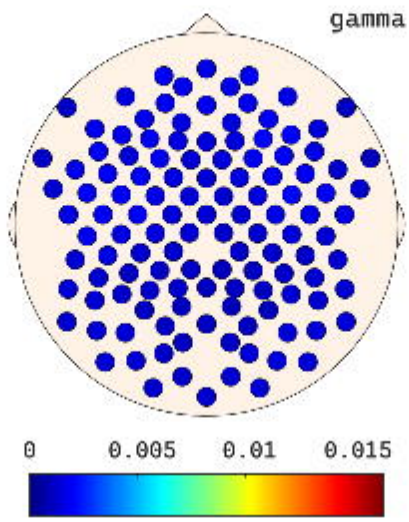
gamma
0
0.005
0.01
0.015

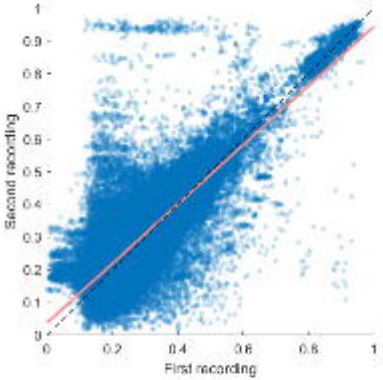
Second recording
First recording

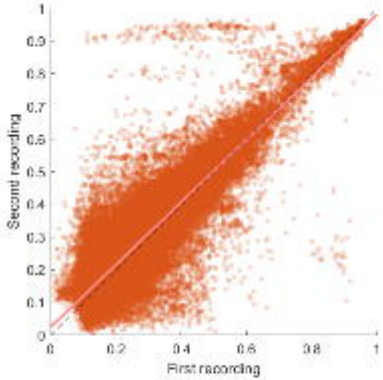
Second recording
First recording

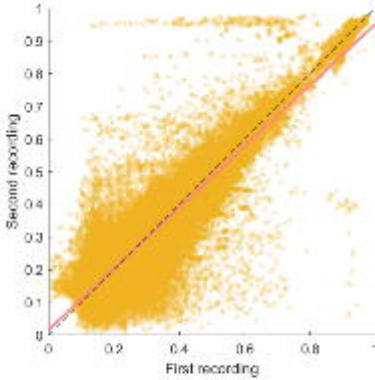
Second recording
First recording

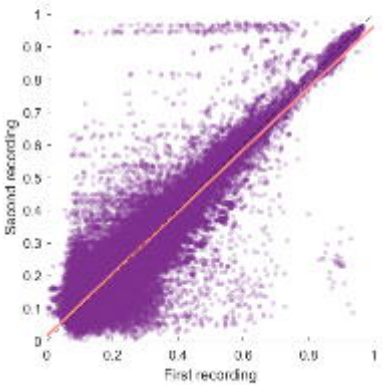
Second recording
First recording

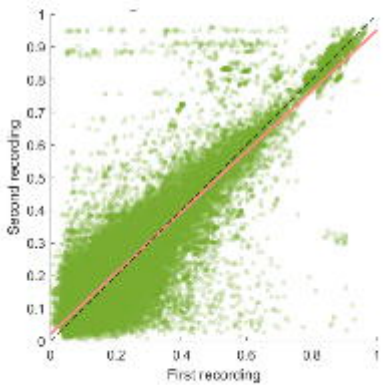
Second recording
First recording

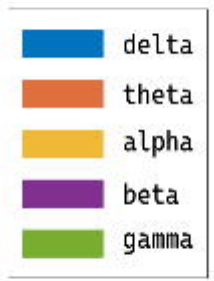
delta
theta
alpha
beta
gamma

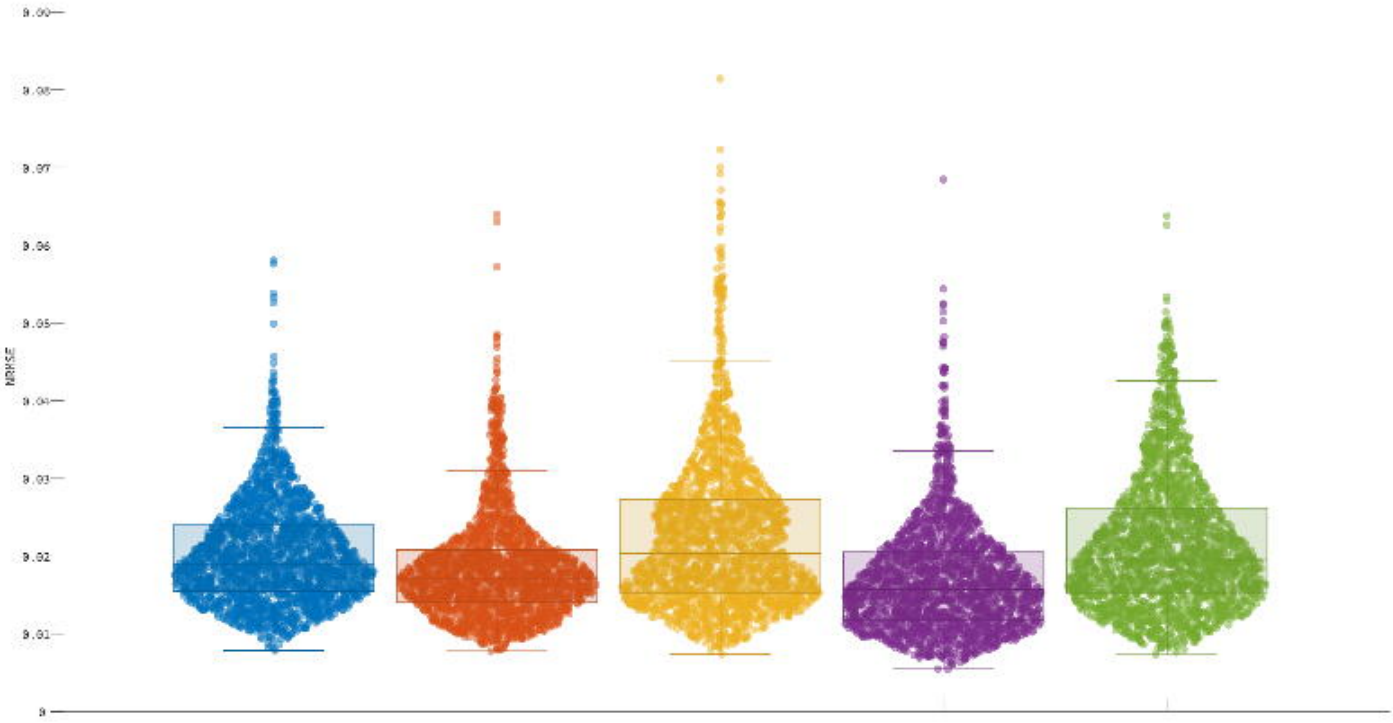
MMSE

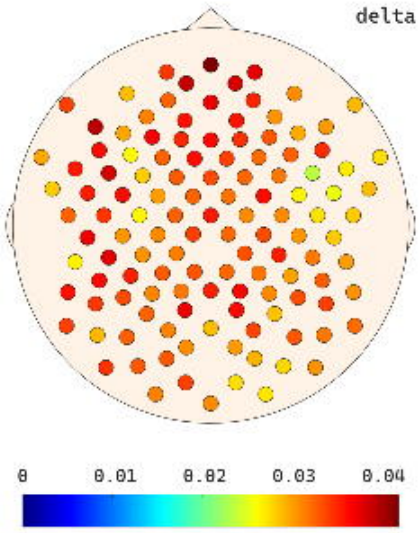
delta
0
0.01
0.02
0.03
0.04

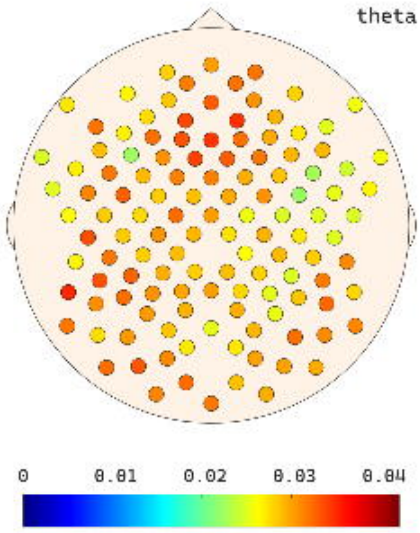
theta
0
0.01
0.02
0.03
0.04

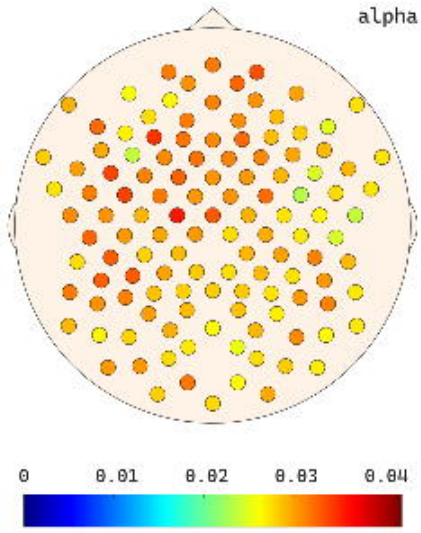
alpha
0
0.01
0.02
0.03
0.04

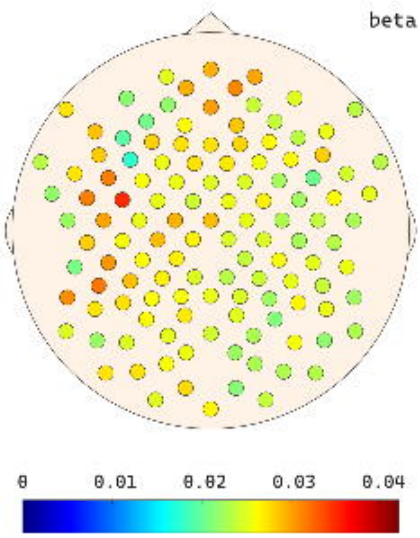
beta
0
0.01
0.02
0.03
0.04

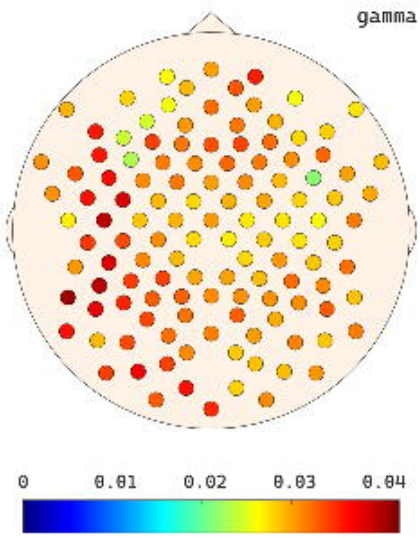
gamma
0
0.01
0.02
0.03
0.04